Universidade de Lisboa
Faculdade de Ciências
Departamento de Física

A 31P MR Spectroscopy Study on Rat Models of Liver Disease

Frederico Ribeiro da Silva Severo

Dissertação
Mestrado Integrado em Engenharia Biomédica e Biofísica
Perfil de Radiacões em Diagnóstico e Terapia

2014

Universidade de Lisboa
Faculdade de Ciências
Departamento de Física

A 31P MR Spectroscopy Study on Rat Models of Liver Disease

Frederico Ribeiro da Silva Severo

Dissertação
Mestrado Integrado em Engenharia Biomédica e Biofísica
Perfil de Radiacões em Diagnóstico e Terapia

Orientador externo: Professor Doutor Maurits Jansen
Orientador interno: Professor Doutor Hugo Ferreira

2014

Resumo

O objectivo deste projecto assenta no desenvolvimento e optimização de técnicas de Espectroscopia por Ressonância Magnética com Fósforo-31 (^{31}P MRS), para a avaliação do conteúdo metabólico e descoberta de biomarcadores em modelos de patologia hepática. A Espectroscopia por Ressonância Magnética é uma técnica não invasiva utilizada para estudos metabólicos, qualitativos e quantitativos. Esta técnica permite, especificamente no caso do Fósforo-31, a avaliação e quantificação de metabolitos cuja composição contenha Fósforo, como é caso da Fosfocreatina, Adenosinatrifosfato ou o Fosfato Monosódico. Através da avaliação qualitativa e quantitativa destes metabolitos há como objectivo a asserção de diversas patologias e alterações metabólicas de forma consistente, segura e não invasiva.

O estudo tem como base a optimização de sequências pré-existentes, como ISIS (Image Selected In-vivo Spectroscopy), CSI (Chemical Shift Imaging) e SPULS (Single Pulse and 1D acquire), assim como o desenvolvimento de uma sequência de localização 1D sem auxílio de gradientes. Esta sequência, denominada SATSP (SATurated Single Pulse), tem como base a sequência SPULS, que consiste na utilização de um único pulso de excitação (*hard pulse*) para a obtenção de informação espectroscópica, acrescentado-lhe um pulso de saturação prévio (neste caso específico baseado na sequência PRESS). O objectivo é proceder à saturação de toda a área não desejada antes da excitação do tecido e aquisição do sinal. O pulso de excitação é então aplicado uniformemente, sendo possível obter sinal apenas da região não saturada. Assim, todo o sinal adquirido terá como origem a área de interesse que, em última instância, deverá corresponder ao fígado.

O projecto inclui o design e posterior utilização de uma fantoma (denominado Liver Phantom) de dois compartimentos cujo objectivo é simular um corte transversal da região abdominal de um rato Sprague Dawley, contendo uma primeira camada simulando pele/músculo/gordura (1º compartimento, com um volume de 10ml situado em contacto com a *surface coil,* contendo Fosfato Dissódico, 40mM), e uma segunda camada simulando o fígado (2º compartimento, com um volume de 35ml, situado do lado oposto à *surface coil,* contendo Ácido Fenil Fosfórico, 10mM). A escolha dos componentes teve como base a sua fácil distinção a nível de frequência de ressonânica (apresentam-se bastante distantes no espectro), e o facto de ambas as substâncias gerarem apenas um pico visível no espectro.

Foram também adquiridos dados experimentais in-vivo (ratos Sprague-Dawley, grupo de controlo n=2, grupo de modelo de doença n=2), os quais foram posteriormente comparados com artigos de referência. Aos ratos pertencentes ao grupo de modelo de doença, administrou-se, por via intraperitoneal, Tetracloreto de Carbono (CCl4) durante um período de 8 semanas, duas vezes por semana,

causando fibrose hepática avançada ou início de cirrose.

Para ambas as situações, in vitro e in vivo, foram descritos protocolos experimentais específicos, que detalham a ordem dos acontecimentos, os métodos de calibração e possibilidades de shimming (manual e automático).

Todos os dados experimentais foram adquiridos especificamente para este projecto, utilizando um scanner pré-clínico de pequeno diâmetro Varian 7T, Surface Coil Tx/Rx Doty30 ($^{1}H/^{31}P$) e software de aquisição vNMRj 3.2, sendo os resultados processados com o auxílio do software jMRUI e Matlab.

Todo o hardware utilizado foi cuidadosamente descrito, começando pelo scanner e os seus vários componentes, até ao material utilizado na preparação da aquisição e durante a mesma. Foram especificadas as diferenças de material utilizado in vitro e in vivo, de modo a estabelecer um contraste de complexidade entre as duas modalidades.

Relativamente à análise dos resultados, o método de processamento de dados utilizado foi o AMARES (Advanced Method for Accurate, Robust and Efficient Spectral fitting), que tem em conta pârametros pré-estabelecidos pelo utilizador. Uma descrição detalhada do método de análise encontra-se disponível nesta dissertação, desde a preparação dos dados, ao nível da correcção de fase, *zero filling* ou truncagem, até à escolha de pârametros a utilizar com o algoritmo AMARES.

No contexto de análise espectroscópica in-vivo ao fígado, e no caso da espectroscopia com Fosfóro-31, foram 6 os metabolitos tidos em conta, nomeadamente Fosfomonoesteres (PME), Fosfodiesteres (PDE), Fosfato Inorgânico (Pi), Adenosina Trifosfato (ATP-α, β, e γ), Fosfocreatina (PCr) e Dinucleótido de Nicotinamida e Adenina (NADH). Variações na concentração e rácios de PDE, PME, Pi e ATP foram previamente referenciadas como possíveis indicadores de alterações patológicas na actividade hepática e, como tal, foram atentamente estudadas.

Os resultados indicaram uma variação no rácio PME/(PME+PDE), denominado Anabolic Charge, entre os dois grupos em estudo. Especificamente, o grupo de controlo apresenta valores de AC mais baixos do que o grupo de modelo de doença. Existe também um aparente decréscimo de concentração absoluta de PDE no grupo de modelo de doença, embora a falta de dados comparativos impossibilite uma maior certeza neste parâmetro . Não foram detectadas variações consideradas significativas no rácio de ATP e Pi.

Foi sugerido o aumento da amostra de ambos os grupos (controlo e modelo de doença) de modo a obter resultados que expressem de uma forma mais segura e significativa as diferenças entre os dois grupos, assim como um estudo

longitudinal que incluísse a recolha histológica de daos em simultâneo com o estudo espectroscópico. A utilização de uma Volume Coil em combinação com a Surface Coil utilizada foi considerada como uma das possíveis mais valias a acrescentar no futuro.

Paralelo ao estudo metabólico previamente descrito foi criado um mapa de Flip Angle para a Surface Coil Doty30, utilizada durante o estudo, o qual evidenciou problemas de alcance e baixa homogeneidade de campo, assim como um estudo inicial de quantificação metabólica absoluta.

O mapa de *Flip Angles* da Surface Coil Doty30 foi criado através do método do rácio do ângulo duplo. Para este médodo são adquiridas duas imagens *Gradient Echo,* a primeira com um flip angle arbitrário *x*, e outra com um flip angle *2x*. Através do rácio entre a magnitude de ambas as imagens adquiridas é possível chegar ao flip angle efectivo aplicado na amostra/tecido/etc. Para estas aquisições foi utilizado um pequeno fântoma de plástico com cerca de 50ml de fosfato monosódico, com concentração 1M. Para a produção do mapa de *Flip Angles* foi desenvolvido de raiz um código *Matlab* que gera automaticamente os mapas, tendo como input as imagens de *Gradient Echo* adquiridas com flip angle x e 2x. O estudo mostrou um curto alcance na aquisição de sinal por parte da surface coil, cerca de 2cm de profundidade, e uma fraca homogeneidade de campo, algo esperado com uma coil deste tipo. Para estudos futuros foi sugerida a utilização combinada de uma volume coil para aplicação dos pulsos RF (maior homogeidade de campo), e uma surface coil para a aquisição do sinal (maior próximidade).

Para o estudo de quantificação metabólica absoluta, foi utilizado um método que envolve a troca do espécime após a aquisição in vivo, e a posterior replicação das condições iniciais para nova aquisição, desta vez utilizando um fântoma com uma concentração fosfórica conhecida. Foi utilizado um fântoma cilíndrico de vidro, com Ácido Fenil Fosfórico, 50mM. Este método foi apenas aplicado a um dos ratos do grupo de modelo de doença, servindo assim como prova de conceito para quantificação absoluta, não tendo havido comparação entre os dois grupos. Os resultados mostraram-se promissores, sendo um dos objectivos futuros a aplicação deste método em todos os estudos em que a quantificação absoluta possa ser benéfica. Como desvantagem, o método descrito implica a repetição das sequências utilizadas in vivo, elevando para o dobro o tempo total de aquisição.

Concluiu-se que a Espectroscopia por Ressonância Magnética se apresenta como uma técnica viável a nível de quantificação metabólica não invasiva.

Palavras-chave: espectroscopia em ressonância magnética com fósforo 31, *saturated single pulse sequence*, *chemical shift imaging*, fibrose hepática, cirrose, biomarcadores de patologia hepática.

Abstract

The overall aim of the project is to evaluate the role of ^{31}P Magnetic Resonance Spectroscopy in preclinical models of liver fibrosis and cirrhosis and to determine the utility of ^{31}P MRS as a non-invasive test for biomarkers. Specifically, two main problems are to be addressed: the possibility of MRS providing reliable information on liver functional status in preclinical models, to the point of rendering multiple time point sampling (biopsy) obsolete; and identifying novel biomarkers that distinguish control and disease model groups. This study includes both In Vitro (with a specific designed liver phantom) and In Vivo data (Sprague-Dawley rats, control group n = 2, disease model group n =2). Several pulse sequences were tested, with more relevance given to CSI (Chemical Shift Imaging) and SATSP (Saturated Single Pulse, a newly made combination of single pulse acquisition with prior use of saturation pulses) sequences. Results show some degree of variation in metabolite ratio between control and disease model groups, specifically with PME and PDE ratios. A bigger sample size for both control and disease model groups is proposed to further verify these claims.

Keywords: 31P magnetic resonance spectroscopy, saturated single pulse sequence, chemical shift imaging, liver fibrosis, cirrhosis, biomarkers of liver disease.

Acknowledgements

A huge thank you to Dr. Maurits Jansen, for teaching me almost everything I know about this subject. For everyone else at the University of Edinburgh, Ross Lennon, Gavin Merrifield, Gregorio Naredo and Ian Marshall.

Thank you Hugo Ferreira, for helping me with my bachelor's dissertation, and once again with this one.

To Marta Ribeiro, designer extraordinaire, who helped me go from a rough sketch of a 2 compartment phantom to a perfectly beautiful (and printable) 3D model, a massive thank you.

Special thanks to Salomé Matos for inviting me to her home and letting me sleep on her couch during the first few weeks of my internship. Edinburgh is a very cold city in February, your heater was nothing short of life-saving.

Thank you Natalia Equihua, José Macena and Dominik Brucher for all the nights we spent having dinner and listening to jazz music. Extra thanks to Natalia for the rainy weekends and homemade Pesto.

To all my friends in London at the time, Ana Figueira, Débora Salvado, João Monteiro, Jo-Anne Tan, and a few others I can't remember right now, thanks for all the technical help, conversations, fun times and general stupidity.

To my very lovely and Indonesian best friend Nabila Wibowo, thank you for keeping in touch almost every day.

To Catarina Freitas, for putting up with me.

And last but never least, I would like to thank my parents, for all the help through the years.

Table of Contents

1. INTRODUCTION 1

1.1 Aim of the work 1
1.2 Dissertation Outline 2

2. BACKGROUND IN MAGNETIC RESONANCE IMAGING 4

2.1 Nuclear Magnetic Resonance 4
2.2 Relaxation Processes and the Bloch Equations 5
2.2.1 Longitudinal Relaxation (T1) 5
2.2.2 Transverse Relaxation (T2) 5
2.3 Chemical Shift 6
2.4 Spin–Spin Coupling 7
2.5 B1 Inhomogeneity and Mapping B1 transmit fields 9
1.6.1 Double Angle (ratio method) 10
2.6 Alternative Nuclei 11
2.6.1 Phosphorous 31 11
2.6.2 Identification of Resonances 12

3. ANIMAL MODELS OF LIVER FIBROSIS 14

3.1 In-Vivo Study 15

4. MR SETUP 17

4.1 The MRI apparatus 17
4.2 Magnet and Gradient 17
4.3 RF Coil 17
4.3.1 Tuning and Matching 20
4.4 In Vivo specific hardware 21

5. MR SPECTROSCOPY SEQUENCES 23

5.1 Image Selected In Vivo Spectroscopy (ISIS) 23
5.2 Single Pulse and 1D acquire (SPULS) 26
5.3 Saturated Single Pulse (SATSP) 27
5.4 Chemical Shift Imaging (CSI) 28
5.5 Gradient Echo (GEMS) 29

6. EXPERIMENTAL PROTOCOLS 30

6.1 Phantom Protocol 30
6.2 In Vivo Protocol 31

7. METHODS OF DATA ANALYSIS 33

7.1 Preparation 33
7.2 Quantification 36
7.2.1 AMARES 37

8. PHANTOM DESIGN 40

8.1 Liver Phantom 40
8.1.1 Concept and early draft 40
8.1.2 Phantom Design and Production 41

8.1.3 Phosphorous Components *45*
8.1.4 Problems and possible solutions *47*
8.2 PPA PHANTOM 49
8.2.1 Phosphorous Components *50*
8.3 FLIPMAP PHANTOM 50
8.3.1 Phosphorous components *51*

9. PHANTOM DATA RESULTS 52

9.1 ISIS 52
9.2 SPULS 53
9.3 SATSP 54
9.4 CHEMICAL SHIFT IMAGING 56
9.5 PHANTOM DATA ANALYSIS 57

10. IN VIVO DATA RESULTS 62

10.1 ISIS 62
10.2 SATSP 63
10.3 CHEMICAL SHIFT IMAGING 65
10.4 IN VIVO DATA ANALYSIS 69

11. ADDITIONAL RESULTS 72

11.1 ABSOLUTE QUANTIFICATION 72
11.1.1 Discussion *75*
11.2 B1 MAPPING 77
11.2.1 Experimental Setup *77*
11.2.2 Experimental Data *77*
11.2.3 B1 Map creation (Matlab Script) *78*
11.2.4 Generated B1 maps *79*

12. GENERAL DISCUSSION 82

13. CONCLUSION 85

14. APPENDIX 86

14.1 SATSP PULSE SEQUENCE 86
14.2 FLIP ANGLE MAP GENERATION IN MATLAB 88

15. REFERENCES 89

Abbreviations and Symbols

AMARES	Advanced Method for Accurate, Robust and Efficient Spectral fitting of MRS data with use of prior knowledge
AMP	Adenosine monophosphate
ADP	Adenosine diphosphate
ATP	Adenosine Triphosphate
B0	Main Magnetic Field (in Tesla)
B1	Magnetic radiofrequency field of the transmitter (in Tesla)
CCl4	Carbon tetrachloride
CSI	Chemical Shift Imaging
DP	Disodium Phosphate
EP	Excitation Pulse
EPI	Edinburgh Preclinical Imaging
FID	Free induction decay
FFT	Fast Fourier transform
FOV	Field of View
GUI	Graphic User Interface
IP	Inversion Pulse
ISIS	Image Selected in vivo spectroscopy
MRI	Magnetic Resonance Imaging
MRS	Magnetic Resonance Spectroscopy
NMR	Nuclear Magnetic Resonance
OVS	Outer Volume Suppression
PCr	Phosphocreatine
PPA	Phenylphosphonic Acid
PPM	Parts per Million
PRESS	Point Resolved Spectroscopy
ROI	Region Of Interest
RF	Radiofrequency
SNR	Signal to Noise ratio
SP	Saturation Pulse
SPULS	Single Pulse and 1D acquire
SPECIAL	SPin ECho, full Intensity Acquired Localized spectroscopy
STEAM	Stimulated Echo Acquisition Mode
SVD	Singular Value decomposition
T1	Longitudinal relaxation time constant (in seconds)
T2	Transverse relaxation time constant (in seconds)
TE	Echo Time (in seconds)
TMS	Tetramethylsilane
TR	Repetition Time (in seconds)

List of Figures

Fig 1 Spin-spin interactions involved with scalar coupling.. 8
Fig 2 Spin Spin coupling in ,1,2-trichloroethane during 1H MR Spectroscopy. 9
Fig 3 Typical localized in vivo ^{31}P NMR spectra from (A) rat skeletal muscle, (B) brain and (C) live. 12
Fig 4 A typical Sprague-Dawley albino laboratory rat 16
Fig 5 Doty Scientific Doty30....18
Fig 6 Remote Coil Matching Units, for both Proton and Phosphorous, from left to right. 19
Fig 7 Rearside view of the magnet hole and a schematic of Varian's High Band RF pre amplifier. 19
Fig 8 Tune Interface Box and Re-Routing Unit representations, from left to right. 20
Fig 9 SA Instruments Inc. (SAII) Model 1025 MR-compatible monitoring and gating system. 21
Fig 10 ISIS pulse program, as seen in vNMRJ 23
Fig 11 Pulse sequence for ISIS localization....24
Fig 12 Experimental evaluation of 2D ISIS localization by MRI 25
Fig 13 SPULS pulse program, as seen in vNMRJ 26
Fig 14 SATSP pulse program, as seen in vNMRJ 27
Fig 15 CSI pulse program, as seen in vNMRJ 28
Fig 16 CSI map and relative anatomical representation. 28
Fig 17 GEMS pulse program, as seen in vNMRJ 29
Fig 18 General view of jMRUI. A CSI sequence is displayed 33
Fig 19 Apodization Toolbox and its effect on the visual representation of a spectrum 34
Fig 20 Phasing Toolbox, showing both Zero Order Phase and Begin Time as flexible parameters. 35
Fig 21 Zero Filling Toolbox, with the number of points to add to the spectrum. 35
Fig 22 Effect of zero filling on spectral resolution 36
Fig 23 A three way view of the AMARES toolbox as presented in jMRUI....37
Fig 24 Example of good data fitting using Amares. Estimated spectrum looks similar to the original one.....38
Fig 25 Example of bad data fitting using Amares. Estimated spectrum barely resembles the original.....38
Fig 26 Early draft of the Liver Phantom....40
Fig 27 First tridimensional draft of the Liver Phantom 41
Fig 28 Left: Tridimensional model of the Liver Phantom. Right: Final, printed version of the Liver Phantom.42
Fig 29 Three-way perspective of the separated small mpartment, after the epoxy resin had been applied.....43
Fig 30 Three-way view of the combined large and small compartment. 44
Fig 31 Final, developed form of the Liver Phantom....45
Fig 32 SCOUT images of a transversal cut of the Liver Phantom with (right) without (left) the air bubble.....47
Fig 33 PPA Phantom in three different perspectives....49
Fig 34 Threeway view of the FlipMap Phantom. 50
Fig 35 ISIS pulse sequence | TR 2000 ms | 256 averages | 25x43x5 mm voxel, positioned inside the second compartment | EP [Hard, 90°, 50 μs, 41 dB] | IP [HS-AFP, 270°, 500 μs, 45dB] | Very high apodization 52
Fig 36 ISIS pulse sequence | TR 2000 ms | 256 averages | 25x43x5 mm voxel, positioned inside the second compartment | EP [Hard, 135°, 50 μs, 45 dB] | IP [HS-AFP, 270°, 500 μs, 45dB]....52
Fig 37 SPULS sequence with a low flip angle, Hard pulse 90° [100 μs, 35 dB] | 16 averages | TR 2000ms | ...53
Fig 38 SPULS sequence high flip angle, Hard pulse 350° [100 μs, 44 dB] | 16 averages | TR 2000ms | 53
Fig 39 SATSP sequence | EP Hard 350° [100 μs, 45 dB] | SatP hs20 90° [2000 μs, 33dB] | 16 averages | TR 2000ms | 54
Fig 40 SATSP sequence | EP Hard 350° [100 μs, 45 dB] | SatP sinc 90° [2000 μs, 22dB] | 16 averages | TR 2000ms | 54
Fig 41 SATSP sequence | EP, Hard 350° [100 μs, 45 dB] | SatP, gauss 90° [2000 μs, 20dB] | 16 averages | TR 2000ms | 55
Fig 42 SATSP sequence | EP, Hard 350° [100 μs, 45 dB] | SatP, Hard 360° [110 μs, 44dB] | 16 averages | TR 2000ms | 55
Fig 43 CSI sequence |2 dummy scans | 32 averages | TR 2000ms | Data Matrix 8x8 |Slice orientation – Coronal, Phase 1d 40mm, 2d 40mm, Thickness 40mm |No saturation bands were used 56
Fig 44 Metabolite Ratio varying on applied Flip Angle 58

Fig 45 DP signal amplitude depending on FA 58
Fig 46 Phenylphosphonic Acid signal amplitude depending on FA 59
Fig 47 Saturated vs Non saturated SPULS 60
Fig 48 DP/PPA ratio with increasing number of averages 61
Fig 49 ISIS pulse sequence | TR 2000 ms | 256 averages | 25x31x5 mm voxel, positioned inside the liver | EP [Hard, 200°, 100 µs, 44 dB] | IP [HS-AFP, 260°, 500 µs, 46dB] 62
Fig 50 Control Group - subject n1| high flip angle 350° [EP [280 µs, 39dB] | 64 averages | SW 8000 Hz | ... 63
Fig 51 Control Group - subject n1| high flip angle 350° [EP [280 µs, 39dB] | 64 averages | SW 8000 Hz | SP [360° Hard, 140 µs, 45dB] 63
Fig 52 Control Group - subject n2| high flip angle 350° [EP [280 µs, 39dB] | 64 averages | SW 8000 Hz | ... 64
Fig 53 Control Group - subject n2| high flip angle 350° [EP [280 µs, 39dB] | 64 averages | SW 8000 Hz | SP [360° Hard, 140 µs, 45dB] 64
Fig 54 Control Group - subject n1 | CSI sequence |2 dummy scans | 64 averages | TR 2000ms | Data Matrix 8x8 |Slice - Phase 1d 60mm, 2d 60mm, Thickness 10mm |No saturation bands were used 65
Fig 55 Control Group - subject n2 | CSI sequence |2 dummy scans | 64 averages | TR 2000ms | Data Matrix 8x8 |Slice - Phase 1d 60mm, 2d 60mm, Thickness 10mm |No saturation bands were used 66
Fig 56 Disease Model group - subject DM1 | CSI sequence |2 dummy scans | 96 averages | TR 2000ms | Data Matrix 8x8 |Slice - Phase 1d 60mm, 2d 60mm, Thickness 15mm |No saturation bands were used 67
Fig 57 Disease Model group - subject DM1 | CSI sequence |2 dummy scans | 96 averages | TR 2000ms | Data Matrix 8x8 |Slice - Phase 1d 60mm, 2d 60mm, Thickness 15mm |No saturation bands were used 68
Fig 58 Red squares depicts voxels with higher total combined acquired signal, while blue (all the way to translucent blue) squares represents those with lower acquired signal. 72
Fig 59 PPA Phantom Voxel label for absolute quantification. 73
Fig 60 Three FlipMap phantom gradient echo images acquired with different number of averages. From left to right, images were acquired with 32, 512 and 1024 averages, respectively. 78
Fig 61 Three FlipMap phantom gradient echo images acquired with different flip angles. From left to right, images were acquired with 20, 40 and 80 degrees, respectively. 78
Fig 62 Generated B1 map without the noise correction algorithm 80
Fig 63 Generated B1 map with the noise correction algorithm. 80

List of Tables

Table 1 Chemical shifts of biologically relevant 31P-containing metabolites. 13
Table 2 Typical values/settings used in each of the AMARES required parameters 38
Table 3 Disodium phosphate characteristics and chemical representation. 45
Table 4 Phenylphosphonic acid characteristics and chemical representation. 46
Table 5 Monosodium Phosphate characteristics and chemical representation. 51
Table 6 Subject DM2 absolute metabolite concentration for each of the 9 considered voxels 74
Table 7 Parameters used in several GEMS image acquisitions. 77

1. Introduction

1.1 Aim of the work

Cirrhosis is a diffuse condition, characterized by extensive fibrosis and nodule formation, vascular distortion and liver cell dysfunction [1]. As a result of alterations in the liver microcirculation mediated by myofibroblast-induced sinusoidal constriction, vascular distortion and shunt formation related to scar deposition, portal hypertension (or PHT) develops in the diseased liver and is responsible for the major clinical sequelae associated with cirrhosis such as ascites, variceal hemorrhage, encephalopathy and renal failure [1][2][3].

In human subjects, and regardless of the cause, patients with chronic liver disease may develop liver fibrosis, which can then progress to cirrhosis. In early stages there are no palpable or clear clinical manifestations of liver fibrosis, a fact that becomes even more complicated if we consider that the clinical manifestations of cirrhosis vary from no symptoms at all to liver failure [4].

Death rates from cirrhosis are increasing rapidly worldwide but, to date, no anti-fibrotic therapies have been approved for use in humans and the standard pharmacological therapy for PHT (non-selective beta blockade) remains unsuccessful in around 60% of patients [2]. While there is an urgent need to develop novel therapies for this problem, it is also required to improve diagnose techniques used to monitor the progression of liver fibrosis and development of PHT (which are highly variable in patients), as well as assess the response and progression related to any interventional approach.

Liver biopsy and hepatic venous portal gradient measurement are still the most used techniques for assessing histology and PHT, respectively, but both are relatively complicated invasive procedures and consequently unsuitable for recurrent analysis of disease parameters in case of a lasting, unpredictable condition. The same limitations apply to animal models, where optimal tests for fibrosis and portal pressure require the killing of animals at serial time points to assess disease progression and severity, instead of allowing a longitudinal assessment in the same animal. As a result of these problems associated with biopsy and other invasive techniques, there has been a steady initiative to find effective non-invasive approaches to evaluate liver damage, including serological tests and several imaging modalities [3]. Still, none of these methods have been universally adopted as of yet and the search for reliable and repeatable biomarkers of disease activity and response to treatment continues. One of these techniques relies on the use of Nuclear Magnetic Resonance (NMR). Two distinct modalities of NMR, Magnetic Resonance Imaging (MRI) and Magnetic Resonance Spectroscopy (MRS), can be used to assess different parameters.

In terms of imaging, In Vivo MRI scanning allows the application of this technique to monitor liver injury in-vivo in clinically relevant animal models [4].

However, there is still minimal data regarding the utility of MRI in animal models of liver fibrosis [4]. The major potential advantage of MRI is that repeated measurements can be made in the same rodent, without killing the animal, thus allowing for a longitudinal assessment of the same animal. The anatomical condition of the affected structures can be evaluated using contrast agents, like gadolinium, or assessing visco-elastic parameters [5], evaluating structural and perfusional abnormalities in the diseased liver in a longitudinal manner (as in human disease). Other indicators of PHT such as splenomegaly, varices and ascites may also be detectable using contrast agents.

When it comes to understanding liver disease in a physiological sense, Phosphorous-31 magnetic resonance spectroscopy (^{31}P MRS) can be used as a non-invasive technique that provides information on hepatic phospholipid metabolism (Adenosine triphosphate, ATP) and hepatocyte energy state (several groups have already tested its use in patients with liver disease and in animal models [6][4]).

Previous studies have shown specific changes in metabolite ratios that are indicative of liver dysfunction, as these pathways are switched into a 'regeneration mode' in an attempt to repair the failing liver [4][7]. However, ^{31}P MR Spectroscopy needs further evaluation in animal models of cirrhosis in a strategic search for novel biomarkers.

The use of ^{31}P MR Spectroscopy has several key elements to be considered in order to get consistent, reliable results, ranging from choosing and optimizing the best possible spectroscopy sequence, improving said techniques for both phantom and In Vivo use, and picking the most appropriate method for data analysis. Inside each one of these there's an infinite amount of possibilities. What kind of phantom should be used? Would it be better to design it from scratch, and if so, what materials can be utilized, what form factor is the most appropriate? Will a standard pulse sequence fulfill our purpose; does it need to be slightly altered? Or does one need to program a totally new one? These are but a few questions intrinsic to the issue at hand.

With all this in mind, one main bullet point to retain is that this body of work will not be focused in one specific part of this process. While most essays tend to center around one particular area of study, be it MR spectroscopy data acquisition, sequence programming or data analysis, it is my intention to go through every step in a manner as meticulous as possible, thoroughly explaining every phase along the way.

1.2 Dissertation Outline

Without getting too much into the basics of magnetic resonance, there is a need for some important concepts to be assimilated before venturing into the actual study. And so, this report will start by describing concepts such as relaxation,

chemical shift or spin-spin coupling.

The next chapter, entitled "Animal models of liver fibrosis" serves both as an explanation of how the condition can be represented and how it translates from the human perspective to the animal model. A specific method to induce liver fibrosis, the CCl4 method, will be detailed.

Then, the MR setup used throughout this study will be carefully described, the various hardware components and combinations documented. Experimental protocols for both in vivo and in vitro follow. In terms of methods of data analysis, both the data preparation, ranging from phasing and apodization to zero filling, and data quantification, which algorithm to use and what parameters were chosen, will be addressed. AMARES, a spectral fitting algorithm with the use of prior knowledge, was used as the primary method of data analysis.

Afterward, all the relevant pulse sequences used during the course of this study are going to be described and detailed. Among this sequences is a custom made Saturated SPULS pulse sequence.

Next, I shall carry on by detailing all the phantoms used during the experiments, putting more emphasis in the creation of a 2 compartment phantom for ^{31}P MR Spectroscopy use, labeled Liver Phantom, from its conceptual stages to its final form and purpose. While not the only phantom used throughout the course of this study, it was by far the most utilized and, as so, deserves a more detailed overview. Two other (more simple) phantoms were used and both their form factors and characteristics will be shortly described as well.

Results are divided into two main sets, Phantom and In Vivo data, with each set split into several sub categories, depending on number of pulse sequences, parameters or subjects/groups in each set. In Vivo and Phantom results are presented separately as a way to address their conclusions, problems and solutions as separate entities. A general discussion is presented afterwards, as a way to compile the general deductions of this study. Some additional results, for absolute quantification and B1 mapping are shown as well, along with specific inferences made from the acquired results.

Finally, a small conclusion will bring this dissertation to an end.

2. Background in Magnetic Resonance Imaging

Nuclear Magnetic Resonance (or simply NMR) techniques involve the manipulation and observation of nuclear magnetic moments intrinsic to matter for generation of an image describing the structural properties of that matter, Magnetic Resonance imaging (MRI), or a spectrum depicting specific compounds present in the scanned sample, Magnetic Resonance Spectroscopy (MRS).

In this section, the physics underlying magnetic resonance techniques is explored. For more information on the topic, a rigorous reference on the subject is provided in *Magnetic Resonance Imaging: Physical Principles and Sequence Design* [8], whilst a more accessible, intuitive discussion may be found in *MRI in Practice* [9].

2.1 Nuclear Magnetic Resonance

Nuclear Magnetic Resonance operates most fundamentally by manipulating spin states of individual nuclei. While it is possible to have an in-depth quantum mechanical description dealing with the statistical distribution of spin states in the material, for the purposes of this report it is sufficient to begin with a classical description describing the net nuclear magnetic moment of the material, as presented in Webb, 1988 [10] and Kuperman and Kuperman, 2000 [11].

As per the classical description, an isolated proton with a charge +e and angular momentum I is initially considered. And so, as described by Maxwell's equations (presented by Maxwell in 1865 [12]), an electronic charge circulating in a conducting loop produces a magnetic field normal to the plane of current rotation. Considering the proton charge to be distributed and rotating along a central axis as a result of the angular momentum, a magnetic dipole moment *mp* antiparallel to the angular momentum vector (and hence, normal to the plane of charge circulation) results, ie, mp = I describes the gyromagnetic ratio, which for the simplified classic model is given by:

$$\gamma = \frac{e}{2m}$$

where m is the proton mass.

An external magnetic flux density B0 will exert a torque T on a magnetic dipole moment, causing the angular momentum to change at a rate equal to the torque, i.e.

$$T = m_p \times B_0$$

$$= \frac{d\mathbf{I}}{dt}$$

And hence,

$$\frac{dm_p}{dt} = \gamma m_p \times B_0$$

The result above is the Larmor equation, which describes the precession of the magnetic dipole moment *mp* about B0 with angular velocity

$$\omega_0 = -\gamma B_0$$

or

$$v_0 = \left(\frac{\omega_0}{2\pi}\right) = \left(\frac{\gamma}{2\pi}\right) B_0$$

In MRI applications, the static, homogeneous B0 field described here is presented by the main field magnet.

2.2 Relaxation Processes and the Bloch Equations

Whereas useful for understanding the MR phenomenon, the classical model presented here cannot explain many features relating to the interactions between nuclei. To overcome some such limitations, a set of phenomenological equations describing the dynamics of nuclear magnetization were proposed in [13].

These Bloch equations describe processes of relaxation of the net magnetization. Various such relaxation processes arise which lead to a fading of the MR signal after the initial excitation; these are largely dependent on the material and structure being observed, and as such their measurement allows characterization of the materials.

2.2.1 Longitudinal Relaxation (T1)

Longitudinal relaxation, also known as spin-lattice relaxation and represented as T1 relaxation, describes the transfer of energy from the spin system, primarily through interactions with adjacent spins in the lattice. This is largely related to mobility and tumbling of molecules in the material – therefore, the physical structure of the material and surrounding surfaces. The T1 relaxation is defined by the Bloch equation

$$\frac{dM_z}{dt} = \frac{M_0 - M_z}{T_1}$$

2.2.2 Transverse Relaxation (T2)

Transverse relaxation, also known as spin-spin relaxation and represented as T2 is loss of net magnetization from the *xy* plane. This is a result of loss of phase coherence due to small variations in the B0 field (and hence, the local

precessional frequency) due to the relationship between the nucleus and the molecular magnetic field, or exchange of spin state between two nuclei. In biological tissue, this process is significantly faster than longitudinal relaxation. Transverse relaxation is described by the remaining Bloch equations,

$$\frac{dM_{xz}}{dt} = -\frac{M_x}{T_2} + \gamma M_y B_0$$
$$\frac{dM_x}{dt} = -\frac{M_y}{T_2} - \gamma M_x B_0$$

In practice, the envelope of the FID is observed to decay at the effective T2 relaxation time T2*, which is always faster than T2. This has the added factor of phase loss due to macroscopic fluctuations due to magnetic field inhomogeneities.

$$\frac{1}{T_2^*} = \frac{1}{T_2} + \frac{\gamma \Delta B_0}{2}$$

When a spin system which has been allowed to dephase for a short period is inverted (perhaps by way of a 180° pulse), the direction of rotation relative to the rotating frame of reference is reversed and the dephased spins begin to rephase. Effects from relatively static macroscopic inhomogeneities (defining T2) are cancelled and an echo signal may be seen from the rephased spin system, attenuated at a rate determined by the T2 component. It is generally this echo signal which is used to produce an image.

2.3 Chemical Shift

Whenever we assume a macroscopic sample containing only one type of nuclear spin, its resonance frequency is solely given by v_0. If this were to be the case MR spectroscopy would be of minor importance in fields such as chemistry or medicine, as you would only be able to identify and quantify each specific chemical element and not distinct compounds with that particular element in it. Nuclei of the same element (or isotope) would resonate at the same frequency because of their identical gyromagnetic ratio. Luckily, however, the resonance frequency ω not only depends on the gyromagnetic ration γ and the external magnetic field *B0,* but it is highly sensitive to chemical environment of the nucleus under investigation [15][16]. This effect is commonly referred to as the chemical shift. This phenomenon is directly caused by shielding (also called screening) of nuclei from the external magnetic field by electrons surrounding them. When placed in an external magnetic field, electrons will rotate about *B0* in an opposite sense to the proton spin precession. Since this precession of electrons involves motion of charge, there will be an associated magnetic moment μ_e, in analogy to the existence to a nuclear magnetic moment. The electron magnetic moment opposes the primary applied magnetic field *B0.*

Therefore, the electrons will reduce the magnetic field that is sensed by the nucleus. This effect can be described in terms of an effective magnetic field B at the nucleus as:

$$B = B_0(1 - \sigma)$$

where σ is the shielding constant. σ is a dimension (normally expressed in parts per million (ppm)), which depends on the chemical environment of the nucleus. And so, the resonance condition can be modified to:

$$v = \left(\frac{\gamma}{2\pi}\right) B_0(1 - \sigma)$$

Chemical shifts are most often not represented in units of Hertz (Hz), as this would make chemical shift value dependent on magnetic field strength. Instead, chemical shifts are expressed in terms of parts per million (ppm). By convention, chemical shift δ is defined as:

$$\delta = \frac{v_{inv} - v_{ref}}{v_{ref}} \times 10^6$$

where V_{inv} and V_{ref} are the frequencies of the compound under investigation and of a reference compound, respectively. The reference compound should ideally be chemically inert and its chemical shift should be independent of external variables (temperature, ionic strength, etc) and more importantly, should produce a strong single resonance signal well separated from all other resonances. Two widely accepted reference compounds for 1H NMR are tetramethylsilane (TMS) and 2,2-dimethyl-2-silapentane-5-sulfonate to which the chemical shift δ = 0 is attributed. Unfortunately, these compounds are nowhere to be found in vivo, making those impossible to use as internal references. In the specific case of in-vivo ^{31}P MR Spectroscopy Phosphocreatine (PCr) tends to be used as an internal reference (0.00 ppm), due to both its widespread presence in the body and relative stability [14].

2.4 Spin–Spin Coupling

The MR resonance frequencies, or chemical shifts, give direct information about the chemical environment of nuclei, thereby greatly aiding in the unambiguous detection and assignment of compounds. The integrated resonance area under each peak is, in principle, directly proportional to the concentration of the compounds, thus making NMR a quantitative technique. An additional feature that can be observed in high-resolution NMR spectra is the splitting of resonances into several smaller lines, a phenomenon often referred to as scalar coupling, J coupling or spin-spin coupling [17]. Scalar coupling originates from the fact that nuclei with magnetic moments can influence each other, besides

directly through space (dipolar coupling) also through electrons in chemical bonds (scalar coupling).

Even though dipolar interactions are the main mechanism for relaxation in a liquid, there is no net interaction between nuclei since rapid molecular tumbling averages the dipolar interactions to zero. However, interactions through chemical bonds do not average to zero and give rise to the phenomenon of scalar coupling.

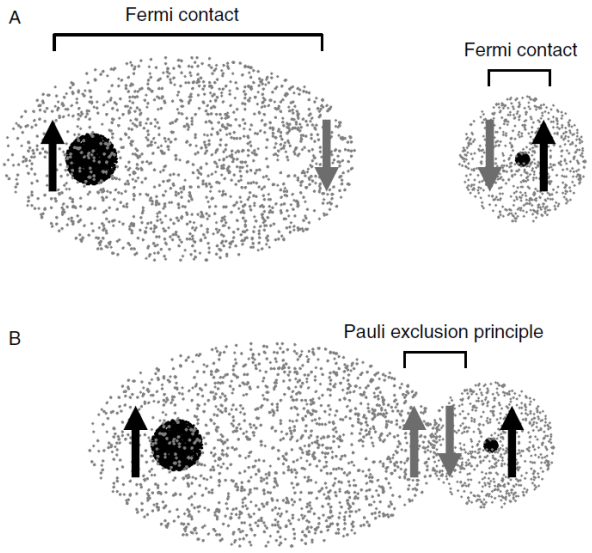

Fig 1 Spin-spin interactions involved with scalar coupling. (A) In isolated atoms, the Fermi contact energetically favors an antiparallel orientation between nuclear and electronic spins. (B) In chemical bonds, the Pauli Exclusion Principle demands that the electron spins are in an antiparallel orientation thereby potentially forcing nuclear and electron spins in an energetically higher parallel orientation, depending on the nuclear spin state [14].

As seen below on Fig 2, illustrating the 1,1,2 trichloromethane example, the H_a and H_b protons are spin-coupled to each other. Starting with the Ha signal, in addition to being shielded by nearby valence electrons, each of the H_a protons is also influenced by the small magnetic field generated by H_b next to it. The magnetic moment of H_b will be aligned with B0 in (slightly more than) half of the molecules in the sample, while in the remaining half of the molecules it will be opposed to B0.

The effective manetic field B 'felt' by H_a is a slightly weaker if H_b is aligned against B0, or slightly stronger if H_b is aligned with B0. In other words, in half of the molecules H_a is shielded by H_b (hence the NMR signal is shifted slightly upfield) and in the other half H_a is deshielded by H_b (and the NMR signal shifted slightly downfield). What would otherwise be a single H_a peak has been split into two sub-peaks (a doublet), one upfield and one downfield of the original signal.

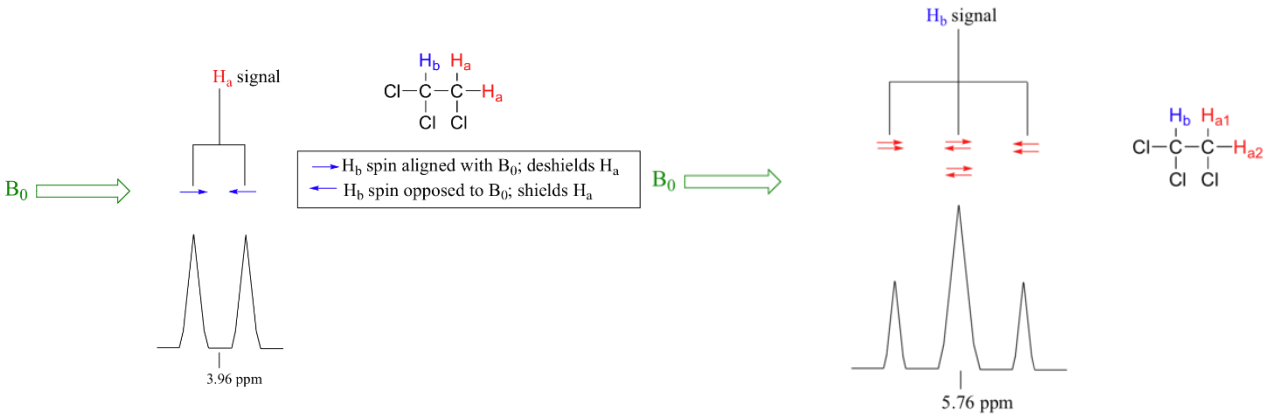

Fig 2 Spin Spin coupling in ,1,2-trichloroethane during 1H MR Spectroscopy [24].

Now let's focus on the H_b signal. The magnetic environment experienced by H_b is influenced by the fields of both neighboring H_a protons, which we will call H_{a1} and H_{a2}. There are four possibilities here, each of which is equally probable. First, the magnetic fields of both H_{a1} and H_{a2} could be aligned with B_0, which would deshield H_b, shifting its NMR signal slightly downfield. Second, both the H_{a1} and H_{a2} magnetic fields could be aligned opposed to B_0, which would shield H_b, shifting its resonance signal slightly upfield. Third and fourth, H_{a1} could be with B_0 and H_{a2} opposed, or H_{a1}opposed to B_0 and H_{a2} with B_0. In each of the last two cases, the shielding effect of one H_a proton would cancel the deshielding effect of the other, and the chemical shift of H_b would be unchanged.

2.5 B1 Inhomogeneity and Mapping B1 transmit fields

It is intuitive that B1 inhomogeneity is a major cause of artifacts in MR imaging modalities. B1 excitation fields are not uniform, particularly with surface coils, multi-coil geometries or high field systems, with one of the direct consequences being degraded SNR. [18].

The signal-to-noise performance of a coil can be improved by reducing the noise volume, which is made possible by placing the coil much closer to the object being imaged; this is one of the basic premises behind the use of surface coils. The reduction in noise volume generally comes at the price of an inhomogeneous B1 field, and hence non-uniformity in the image intensity. In high-field (3T) abdominal, cardiac, and neuro-imaging, *B*1 inhomogeneity on the order of 30–

50% has been predicted and observed [19][20]. This factor can be of extreme importance when considering the use of magnetic resonance spectroscopy.

Directly imaging the flip angle can be hard because there are unknowns such as receive sensitivity and proton density. There are several existing *B*1 mapping methods based on measurements at progressively increasing flip angles [21], stimulated echoes [22], or signal ratios [23]. Still, probably the most simple and straightforward of all these is the double-angle method, which involves acquiring images with two flip angles α and 2α, where TR *T*1 such that image signal is proportional to sin(α) and sin(2α), respectively. The *B*1 field is then derived from the ratio of signal magnitudes [8].

1.6.1 Double Angle (ratio method)

By acquiring two gradient echo images with flip angles α and 2α, with all other signal affecting sequence parameters kept constant, two different images are produced with signal intensity defined by:

$$M_{xy1} = M_0 \sin(\alpha)$$

$$M_{xy2} = M_0 \sin(2\alpha)$$

Taking the ratio removes the M0 dependence. Using sin (2α) = 2cos (α) sin (α),

$$\frac{M_{xy2}}{M_{xy1}} = \frac{2\cos(\alpha)\sin(\alpha)}{\sin(\alpha)}$$

$$\alpha = \cos^{-1}\left(\frac{M_{xy2}}{2\,M_{xy1}}\right)$$

One problem with the double angle method is that the longitudinal magnetization must recover nearly to equilibrium or there will be T1 weighting from the leftover longitudinal magnetization. A long repetition time is typically used with the double-angle methods to ensure that there is no *T*1 dependence in either M_{xy1} or M_{xy2} [9]. To circumvent this issue a magnetization reset sequence after each data acquisition can be applied (with the goal of putting the spin population in the same state regardless of whether α or 2α excitation was used)[8].

GE (Gradient Echo), an echo signal generated from free induction decay by means of a bipolar switched magnetic gradient. The echo is produced by reversing the direction of a magnetic field gradient or by applying balanced pulses of magnetic field gradient before and after a refocusing RF pulse so as to cancel out the position dependent phase shifts that have accumulated due to the gradient.

In the latter case, the gradient echo is generally adjusted to be coincident with the RF spin echo. When the RF and gradient echoes are not coincident, the time of the gradient echo is denoted echo time (TE) and the difference in time between the echoes is denoted time difference.

Gradient echo does not refocus the effects of main field inhomogeneity and therefore is generally used with a short echo time. Disadvantages of gradient echo imaging are compromised anatomic details and artifacts in regions with varying susceptibility e.g. between the air-containing sinuses and brain and especially between hemorrhages and normal tissue.

2.6 Alternative Nuclei

The simplest most widely used nucleus to be considered is the single proton, ^{1}H. Nevertheless, similar principles may be applied to imaging or spectroscopy using various other, more complicated, nuclei, such as Carbon (^{13}C), Phosphorous (^{31}P), Fluor (^{19}F) or Sodium (^{23}Na).

While the quantum mechanical behavior may be more complicated, the behavior of the net magnetic moment in these cases works in a similar fashion, where only the change in Larmor frequency (usually lower than for ^{1}H) needs to be considered. Whereas ^{1}H imaging typically gives the strongest signal (being the most sensitive and abundant nuclei in biological tissue due to the large proportion of water), other isotopes may provide more useful measurements for particular tissue types in certain applications, for either imaging or spectroscopy purposes.

2.6.1 Phosphorous 31

The successful use of proton MR spectroscopy in clinical settings is only matched by ^{31}P MRS [14]. Both its relatively high sensitivity (about 7% of protons') and a 100% natural abundance allow the acquisition of high-quality spectra without the need for long scanning sessions.

The chemical shift dispersion of the phosphates found in vivo is relatively large (around 30 ppm), which means an excellent spectral resolution even when using low (clinical) magnetic field strengths.

2.6.2 Identification of Resonances

Phosphorous NMR spectra from tissues in-vivo typically hold a limited number of resonances. The exact chemical shift position of almost all resonances is sensitive to physiological parameters like intracellular pH and ionic strength. By convention, the PCr (phosphocreatine) resonance is used as an internal chemical shift reference and has been assigned a chemical shift of 0.00 ppm (just as Tetramethylsilane, TMS, in conventional 1H MRS).

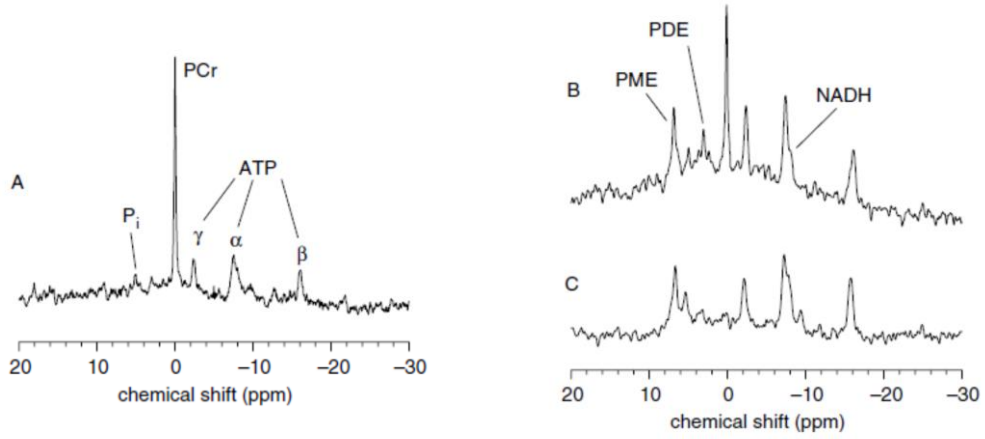

Fig 3 Typical localized in vivo ^{31}P NMR spectra from (A) rat skeletal muscle, (B) brain and (C) liver. Note the complete absence of PCr in the liver [14].

Probably the most important phosphorous based metabolite for gathering information on hepatic phospholipid metabolism is Adenosine Triphosphate. ATP consists of adenosine - composed of an adenine ring and a ribose sugar - and three phosphate groups (triphosphate). The phosphoryl groups, starting with the group closest to the ribose, are referred to as the alpha (α), beta (β), and gamma (γ) phosphates. ATP is highly soluble in water and is quite stable in solutions between pH 6.8–7.4, but is rapidly hydrolysed at extreme pH. At a pH of 7.2, the resonances of ATP appear at -7.52 ppm (α), -16.26 ppm (β) and -2.48 ppm (γ) [14]. Other phosphorous based metabolites are also very well documented.

Below, Table 1 below summarizes the most common metabolites found in ^{31}P MR spectra, as well as its correspondent chemical shifts (referenced relative to Phosphocreatine at 0.00ppm).

Metabolite		**Chemical Shift (ppm)**
Adenosine monophosphate (AMP)		6.33
Adenosine diphosphate (ADP)	α	-7.05
	β	-3.09
Adenosine triphosphate (ATP)	α	-7.52
	β	-16.26

	γ	-2.48
Dihydroxyacetone phosphate		7.56
Fructuose-6-phosphate		6.64
Glucose-1-phosphate		5.15
Glucose-6-phosphate		7.20
Glycerol-1-phosphate		7.02
Glycerol-3-phosphorylcoline		2.76
Glycerol-3-phosphorylcethanolamine		3.20
Phosphomonoester (PME)		6.90
Phosphodiester (PDE)		2.20
Inorganic Phosphate		5.02
Phosphocreatine		0.00
Phosphoenolpyruvate		2.06
Phosphorylcoline		5.88
Phosphorylethanolamine		6.78
Nicotinamide adenine dinucleotide (NADH)		-8.30

Table 1 Chemical shifts of biologically relevant 31P-containing metabolites in no specific order [4][14][42][43].

3. Animal Models of Liver Fibrosis

Animal models of hepatic fibrosis provide a means to study liver degradation and recovery, as seen in numerous studies [25][26][27] . For this to be possible, several approaches to induction of fibrosis have been described [28][29][30], out of which CCl4 (or Carbon tetrachloride) intoxication in rats and mice is probably the most widely studied. In addition, the CCl4 model is the best characterized with respect to histological, biochemical, cell and molecular changes associated with the development of fibrosis [31].

CCl4 can be given IP (Intra Peritoneal) or by oral gavage and it induces zone III necrosis and hepatocyte apoptosis with associated hepatic stellate cell activation and tissue fibrosis [28]. With repetitive dosing, CCl4 can be used to induce bridging hepatic fibrosis (4 weeks of 2 x weekly dosing), cirrhosis (8 weeks of 2 x weekly dosing) and advanced micro-nodular cirrhosis (12 weeks of 2 x weekly dosing). In addition, for each of these models spontaneous recovery from fibrosis can be studied after cessation of dosing [31].

Animal models are essential to the investigation of liver fibrosis and other fibrotic diseases because they provide the only model in which the serial sampling of tissue can be made which facilitate the dissection of the cell and molecular processes that underlie fibrosis. Still, the importance of studying human models of disease cannot be stressed enough. Nevertheless, at best they can only provide a momentary snapshot of a disease process which may develop over weeks or months. In addition, the morbidity, potential mortality and ethical issues associated with liver biopsy in humans, significantly limits the use of biopsy material for research. It's ethically impossible to manipulate the pathogenic process of liver fibrosis experimentally and in vivo in human beings. For all these reasons, animal models of liver fibrosis remain a vital experimental instrument. Many experimental models of hepatic fibrosis have been described, including those associated with toxic damage [28], immunological damage [32], biliary fibrosis [33], and alcoholic liver disease [34].

In a simple way, carbon tetrachloride is a halokane activated by oxidases to yield a trichloromethyl radical, which initiates lipid peroxidation (a process of degradation) and can react with the sulphydrol group of proteins [31]. CCl4 has been administered to rodents by inhalation, gastric gavage and by subcutaneous and intraperitoneal injections [28]. Because of the necessity for bioactivation, the severity of CCl4 injury will be strongly influenced by the type of diet and the presence of other xenobiotics. Consequently, specific diet or drugs can enhance CCl4 toxicity and the speed of development of fibrosis.

Carbon tetrachloride induced fibrosis and cirrhosis is one of the oldest and is probably the most widely used toxin-based experimental model for the induction of fibrosis. It has the advantages that it has been clearly characterized and, in many respects, mirrors the pattern of disease seen in human fibrosis and cirrhosis associated with toxic damage [31]. In addition, there is extensive experience with this model with respect to the characterization of histological, biochemical changes and changes associated with injury, inflammation and fibrosis [28][31]. Finally, in experienced hands, even using outbred rats or mice, this model elicits a reproducible and predictable fibrotic response, making it a valuable basis for study. For these reasons, there is a fairly extensive experience and growing literature in which CCl4 induced fibrosis is used as a basis for mechanistic study.

The CCl4 model also has disadvantages. In comparison, as a model, while mimicking the before mentioned disease pattern it has no direct human disease equivalent. Additionally, unlike human liver fibrosis, there is more pronounced cholangiolar cell hyperplasia in advanced CCl4 fibrosis and in rats in the presence of CCl4 induced cirrhosis there is failure to progress to the development of hepatocellular carcinoma [35][36].

Some groups at the University of Edinburgh have previously used CCl4 in a series of experimental models of liver injury and fibrosis. These include using CCl4: To induce acute injury characterized by self-limiting hepatic stellate cell activation and hepatocellular regeneration; to develop early and established fibrosis (4 to 6 weeks of CCl4), to develop early reversible cirrhosis (8 weeks of CCl4 intoxication) and to develop cirrhosis that demonstrates only partial reversibility (12 weeks CCl4 intoxication) [37][38][39][40].

3.1 In-Vivo Study

For this study, 2 groups of rats were used (control and disease model), all of the Sprague Dawley stock, like the one on Fig 4 . The Sprague Dawley rat is an outbred (bred from distantly related or unrelated individuals, often producing a hybrid of considered superior quality) multipurpose breed of albino rat used extensively in medical research [4][5][31][38]. Its main advantage is its calmness and ease of handling. This breed of rat was first produced by the Sprague Dawley farms (later to become the Sprague Dawley Animal Company) in Madison, Wisconsin in 1925. The average litter size of the Sprague Dawley rat is 11. Each group (control and disesase model) consisted of 2 rats (meaning 4 in total).

Fig 4 A typical Sprague-Dawley albino laboratory rat [41]

Our disease model group was subjected to 8 weeks of twice-weekly intraperitoneal CCl4 which usually induces advanced liver fibrosis or early cirrhosis.

Phosphorous MRS offers a non-invasive technique for studying metabolic processes in the liver. There are mainly six resonances of interest in in vivo liver spectroscopy, namely phosphomonoesters (PME), inorganic phosphate (Pi), phosphodiesters (PDE), and adenosinetriphosphate (alpha, beta, gamma ATP). Resonances from PME and PDE are thought to reflect the cell turnover of the hepatocytes whereas the alpha, beta and gamma groups of ATP reflect the energy state in the cells [42].

In a typical ^{31}P MR spectrum from normal liver tissue low concentrations of PMEs and high concentrations of PDEs have been observed, whereas in fibrotic/necrotic/tumorous tissue elevated levels of PMEs and decreased levels of PDEs have been shown [4][43]. A ratio between these two metabolites has been suggested as a natural biomarker for these conditions, and as such it's going to be one of the focus of the analysis later on.

Other studies [4][7], involving partial hepatectomies, advocate changes in the Inorganic Phosphate/ATP ratios, suggesting an increasing consumption of ATP while the liver tries to compensate by adjusting the liver function. While not directly comparable, it's still worth mentioning.

4. MR Setup

The MRI instrument has evolved into one of the most complex and expensive devices used in imaging practice. Advances in the instrumentation have been the single most important factor in the progress of clinical MRI. This progress can be seen in every hardware field, from advances in magnetic field strength or gradient coil technology, to RF electronics and computer systems.

In principle, the component requirements for an MRI instrument are quite simple. The hardware comprises a magnet to generate a static magnetic field, gradient coils for spatial encoding, RF electronics for irradiation and reception, and computers for data processing and manipulation.

4.1 The MRI apparatus

According to the manufacturer Agilent, the 7T animal MRI system is a flexible and adaptable magnetic resonance imaging scanner for pre-clinical imaging and research. The system has an intuitive user interface (vNMRj), and a flexible programming environment which can carry out a wide range of pre-clinical imaging functions. It was designed with preclinical use in mind.

The high magnetic field provides structural and functional images with higher resolution in comparison with clinical MRI. It is recommended for abdominal, cardiovascular, muscular and articular use, as well as dynamic molecular imaging.

4.2 Magnet and Gradient

The magnetic resonance effect requires the application of a strong homogeneous static magnetic field, which, nowadays, is usually achieved with the use of a superconducting magnet, cooled to cryogenic temperatures during operation. In its superconducting state the wire can conduct much larger electric currents than ordinary wire, creating intense magnetic fields, in our case 7 Tesla.

The gradient used during all experiments was Varian's 205_12_HD. It is described by the manufacturer as a fully self-shielded gradient system designed to suit ≥ 210mm room temperature bore superconducting magnets and gradient systems. The design incorporates fully optimized X, Y and Z coil configurations. The X and Y coils are made from copper plates. The Z coil is wound from heavy duty copper strip. The gradient has been optimized to allow for high duty cycle experiments while the room temperature shim set has been specially designed to minimize coupling between gradients and shims during pulsing. Finally, the gradient set is fully vacuum impregnated to minimize mechanical vibration and noise.

4.3 RF Coil

Radiofrequency (RF) coils are an essential component of what makes up a

complete NMR system. While the magnet creates the spin population difference and therefore the longitudinal magnetization, it is the transverse magnetic field oscillating in the RF range that rotates the longitudinal magnetization into the transverse plane, where it can be detected as an induced signal by a receiver coil. The many different possibilities for RF coil design can partially be explained by the fact that each coil is often a compromise between its desirable and undesirable features, with a general single coil optimal for all applications being no more than a distant utopia. While a volume coil provides a homogeneous B1 magnetic field, such that spin excitation is uniform across the sample, its large size and often poor filling factor compromises their sensitivity. On the other hand, surface coils are very sensitive due to their high filling factor and their optimal size relative to the subject under investigation. However, surface coils have their downsides, in that the generated B1 field is extremely inhomogeneous which will lead to signal loss when an RF pulse is transmitted. Surface coils become advantageous for MR when sample losses are dominant and/or the region of interest is quite close to the surface. A small surface coil will be superior to a well optimized birdcage type-coil when used for features within a few millimeters of the surface. At greater depths, the small birdcage has higher SNR in addition to its strong advantage in RF homogeneity. Here, *coil* (not sample) losses are dominant for both the surface coil and the birdcage, but the surface coil achieves higher SNR over a small region near the surface because of its higher filling factor. The specific coil used in this project is of the $^{1}H/^{31}P$ transmitter/receiver surface coil variety.

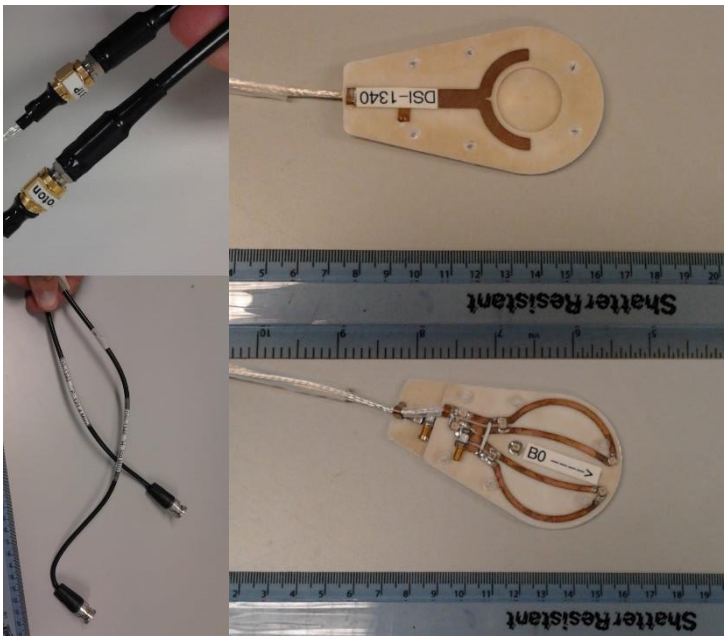

Fig 5 Doty Scientific Doty30

Throughout this study, the coil used was a Doty Scientific *Doty30*, a 30mm diameter $^{1}H/^{31}P$ Double-tuned loop/butterfly surface coil for 7T (Tuned to 1H at 300 MHz, ^{31}P at 122 MHz).

A pair of back-to-back D coils (also called a butterfly coil) can be used to generate an RF magnetic field just below their surface that is orthogonal to that of the loop surface coil and, for proper orientation of the D coils, is also orthogonal to B0 [19, 31]. Hence, the combination of the loop and pair of D coils, as shown in Fig 5, can be used for circular polarization, which may improve SNR [43]. The loop/D combination is also often used for double resonance (e.g., $^{1}H/^{31}P$, or $^{1}H/^{19}F$). In many cases, it permits higher S/N at both frequencies than the alternative of double-tuning a single loop. Alongside the combined $^{1}H/^{31}P$

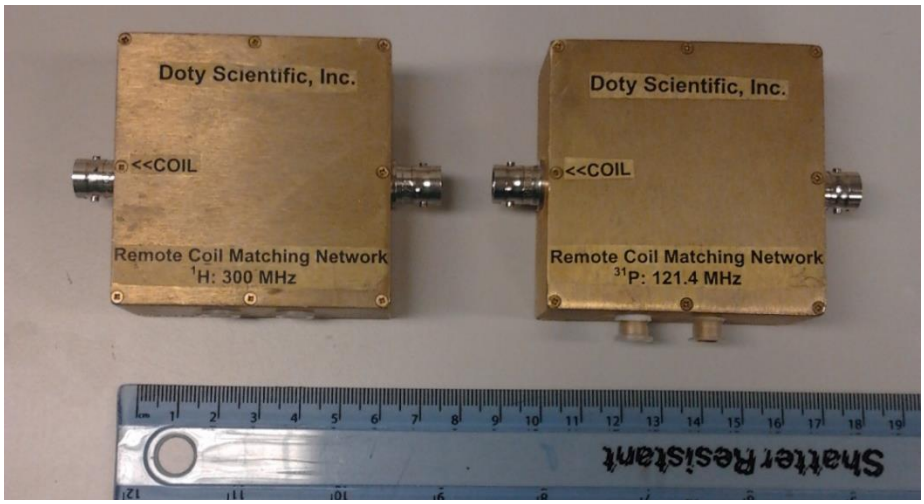

Fig 6 Remote Coil Matching Units, for both Proton and Phosphorous, from left to right. These units were used to manually adjust both matching and tuning on each coil, without the need to access it directly.

surface coil, two remote coil matching networks were used, one for each channel. These boxes allow for remote impedance matching and limited (2%) frequency tuning of the respective surface coils.

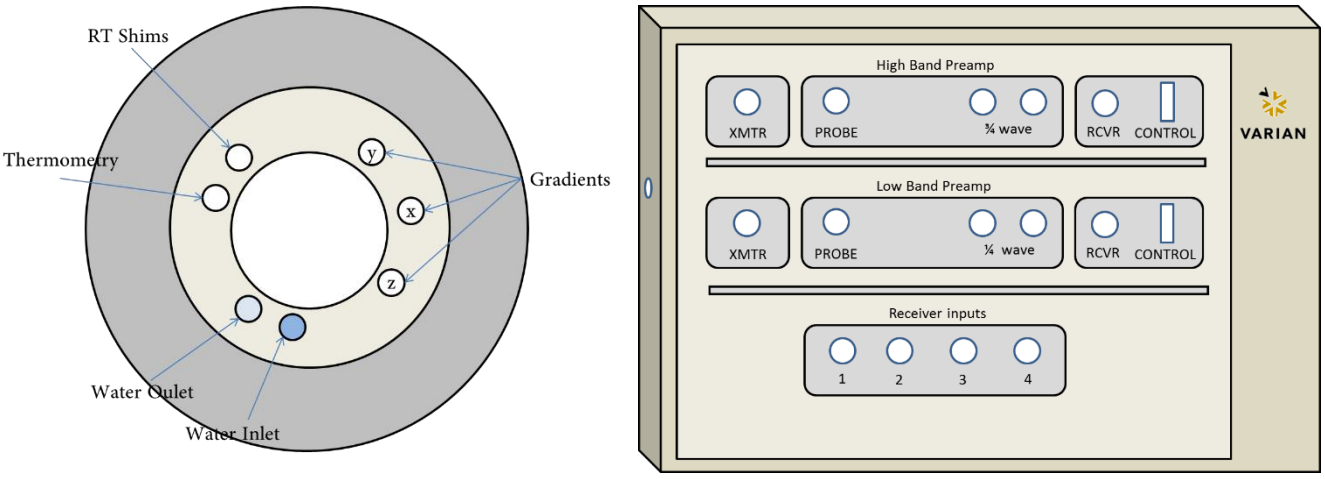

Fig 7 Rearside view of the magnet hole and a schematic of Varian's High Band RF pre amplifier.

4.3.1 Tuning and Matching

In order to be effective for both imaging and spectroscopy, the RF coil must be tuned to resonate at the Larmor frequency f0 of the nucleus to be detected (which in turn will depend on the magnetic field strength [44]). This is usually achieved by adding capacitive or inductive elements across or along the coil structure. Also of great significance is the interface between the coil and the RF hardware of the MRI machine. In order to further minimize losses, optimize power transfer to the coil and suppress reflected signals which may degrade the acquired image or spectra, it is necessary that the impedance of the RF power amplifier, the receiver preamplifier, the cable connecting the coil, and the load presented at the end of the cable are all matched. This tuning and matching is done on a case by case basis, as it depends on the size, shape and composition of the subject being scanned. Connected to the MRI Preamplifier is a tune interface, which can be

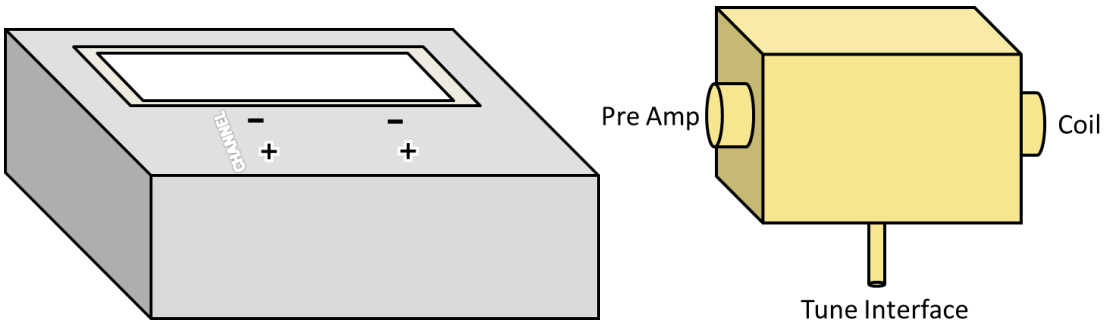

Fig 8 Tune Interface Box and Re-Routing Unit representations, from left to right. The Tune Interface Box was used to check the tuning for each nuclei, the lower the value on the display, the better. The Re-Routing Unit was used to link the coil to the Preamplifier while connecting it to the Tuner.

used by means of re-routing the cables that connect the RF Coil to the pre amplifier (*Fig 7*). This is done using the small apparatus depicted in *Fig 8*.

After the cables are re-routed, the user can tune the coil through the remote coil matching networks (one for each channel). Now, there two approaches as to how the user can monitor if matching/tuning is improving while it's being adjusted. One way to do it relies on the tune interface, which displays a specific value for each channel. The idea is to get this value as low as possible. Another method relies on the software's built-in Probe Tuning mechanism (accessed by typing *mtune* in vNMRj's command window).

When the probe is properly tuned and matched, the tune signal is collinear with the vertical green line and its tip is as close to the baseline (horizontal axis) as possible. Either way, this process had to be done for both the 1H and 31P channels , as both act individually and have different characteristics altogether.

4.4 In Vivo specific hardware

As stated before, this study includes MR scanning sessions done both with phantoms and In-Vivo subjects, and while the basic setup is mostly the same in these two cases, the are some small additions to the hardware department in the In-Vivo case. With the inclusion of a living subject a lot more variables come into play, such as temperature, anesthesia delivery, heart/respiratory rate, as well as the respective gating, meaning the experimental setup is not as straightforward as the one typically used for phantoms.

Animal physiologic monitoring and gating control is provided through a SA Instruments Inc. (SAII) Model 1025 MR-compatible monitoring and gating system. The system can simultaneously monitor and record ECG, respiration, temperature, and blood pressure, depending on the desired parameters and sequences being used.

Fig 9 *SA Instruments Inc. (SAII) Model 1025 MR-compatible monitoring and gating system.*

According to its manufacturer, this system was designed specifically to meet the physiological monitoring and gating needs for anesthetized mice, rats and larger animals in the MR environment. It consists of an ERT Module located near the animal and an ERT Control/Gating Module connected to a PC located near the operator console. The PC displays multiple waveforms, measured values, trends and gating pulses. The ERT Module measures ECG using three leads with needle or surface electrodes, respiratory rate from a small pneumatic pillow sensor and/or from the movement of one ECG lead and temperature with a small rectal thermister probe. Power is supplied by an external, rechargeable battery. The ERT Control/Gating Module receives data from the ERT Module and any of several optional acquisition modules. The ERT Control/Gating Module sends data to the PC for display and receives user instructions from the PC to control measurement and gating functions. Gates from ECG, respiration and any of the available options are generated by the ERT Control/Gating Module

microprocessor and sent to the MR system. The delay from the R-wave peak to the MR system gate is user selectable as is the expiration gate delay and width.

To achieve good results during in-vivo experiments, be it structural, spectroscopic or some other modality, it is absolutely necessary for the animal to be as still as possible inside the scanner. For this to happen, the subject (in this specific case, a rat) is put in a special structure (to put it more precisely, an MR compatible animal holder) and kept under anesthesia.

Regarding the animal holder, a standard RAPID biomedical animal holder was used. RAPID Biomedical offers a variety of animal holders for MRI on both mice and rats. All holders are equipped with nose cones and anesthesia gas delivery. The standard RAPID Animal Holder is also equipped with integrated stereotactic head fixation system, indispensable for things such as high resolution brain imaging. The holders have a length of 870 mm and are prepared to fit standard Tx coils.

The MRI anesthetic apparatus used throughout this study was the Pneupac880. As described by the manufacturer, it comprises a compact, mobile unit specifically designed to be compatible within strong magnetic fields, such as the ones present in a MRI suite, suitable for use in cases of difficult access to the subject (it is designed to work within one meter of the ISO center of the magnet). As a matter of curiosity, this specific device has CE Mark (MDD, Medical Devices Directive) clearance but is has not been approved by the FDA, meaning that it can't be sold or used in the USA.

Another part of the experimental In-Vivo setup is the heater/fan modules. According to the manufacturer's brochure, the SA Instruments, Inc. MR-compatible, small rodent Heater System controls the temperature of small animals undergoing imaging procedures. As referenced above, animal temperature is measured with either a MR-compatible thermister probe. Dedicated software continuously processes the temperature measurements and sends an optical control signal to the Heater Module. This way, the rate of change of temperature is monitored and heater control is adjusted to minimize overshoot and generate a closed loop control system. Mouse temperature variations of less than 0.1°C can typically be obtained during MR examination, providing a great degree of control. This is a very important factor, as the subject's heart rate is dependent on its body temperature [47].

All laboratory work was executed while wearing clean gown and shoes, as well as a disposable mask, mob cap and gloves when required.

5. MR Spectroscopy Sequences

Data acquisition is essentially the be-all and end-all part of the process. Without a good acquired dataset it is impossible to do a reliable analysis and subsequent investigation. Choosing the correct pulse sequence and its parameters is no easy task, as the possible combinations are as numerous as they are complex. There are plenty of factors that come in to play, each with its own advantages and disadvantages, making the process of optimization often difficult and time consuming.

In a very broad general sense there are two fundamentally distinct ways one can approach this subject: localized spectroscopy and non-localized spectroscopy, both with its advantages and disadvantages. Pulse sequence names (and occasionally even specific characteristics) tend to vary between different NMR manufacturer brands, which may cause some confusion to people used to one specific brand and its set of sequences. Keeping in mind that the whole study went down in a Varian/Agilent environment, I'll continue by detailing all pulse sequences considered during the course of this study.

In regards to the Non-Localized Spectroscopy side of things, the very simple SPULS (single pulse and 1D acquire) sequence was put into consideration. Later on this sequence was slightly modified and evolved into a custom made sequence labeled SATSP (SATurated Single Pulse) to fit a saturation pulse prior to excitation, as it will be discussed shortly.

A description of each pulse sequence along with its characteristics follows.

5.1 Image Selected In Vivo Spectroscopy (ISIS)

ISIS is a localization technique that achieves full 3D localization in eight scans, and its basic sequence structure is as shown below in Fig 10.

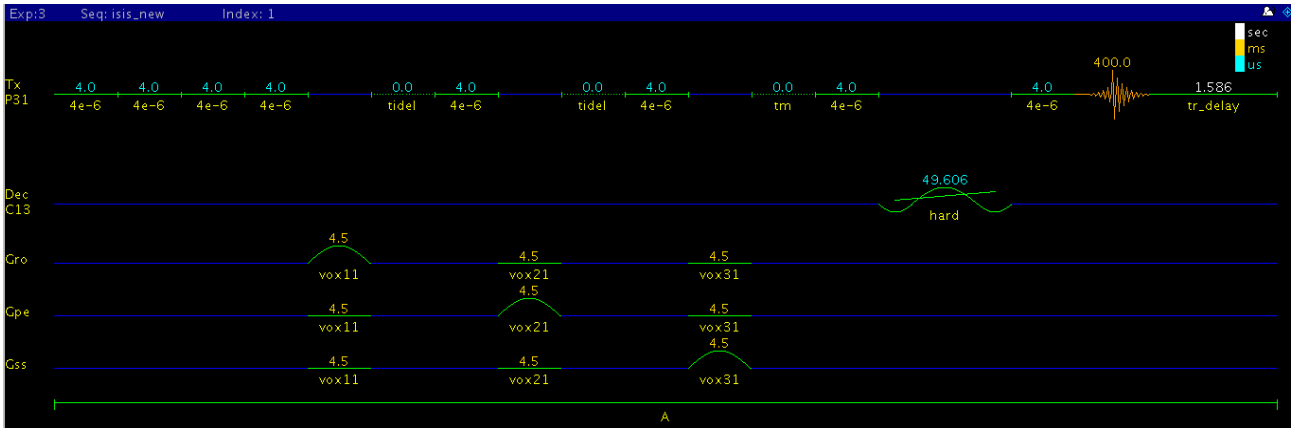

Fig 10 ISIS pulse program, as seen in vNMRj

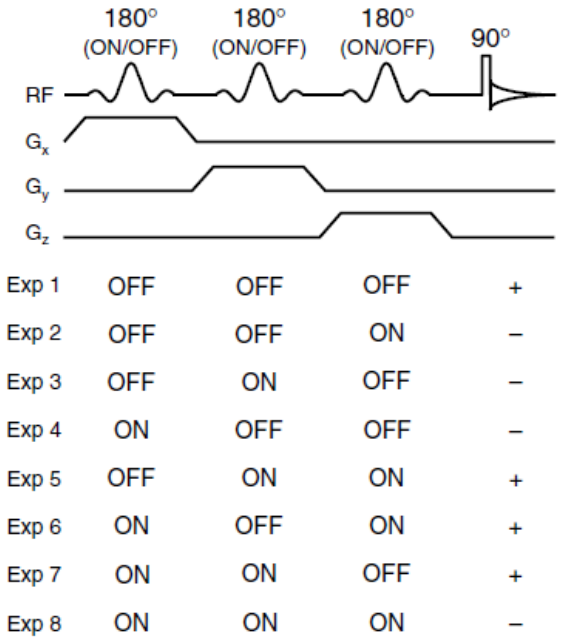

Fig 11 Pulse sequence for ISIS localization. For 1D ISIS localization, two experiments are required, one with and one without a spatially selective inversion pulse prior to excitation. Subtraction of the two datasets will only give signal from the localized volume. For 3D localization, eight experiments (2 × 2 × 2) are required as shown, whereby the right column indicates the relative receiver phase (+ = 0◦, − = 180°) [14]

ISIS uses three frequency-selective inversion pulses in the presence of three orthogonal magnetic field gradients.

These inversion pulses are turned on and off according to an encoding scheme depicted in the above figure. When zero or an even number of 180° pulses are executed, the desired magnetization of the cross-section of the three selected slices ends up along the positive longitudinal axis and following a 90° -x excitation pulse will end up along the positive y axis. During a scan with an odd number of 180° pulses, the desired magnetization ends up along the negative longitudinal axis an is excited to the negative y axis by a 90° -x pulse. Adding and subtracting the individual stored scans with even and odd number of 180° pulses, respectively, will constructively accumulate signal from the desired location while destructively cancelling signal from all other locations, as shown in

Fig 12. In each scan, signal from the entire sample is excited, and the ISIS inversion pulses change the phase of the excited signal. In this case, the scan with two 180° magnetic pulses, the magnetization in the cross section experiences a double inversion and therefore ends up with a positive phase. Then, the localized volume is obtained by subtracting images B and C from images A and D (meaning, final image (F) is obtained by F=A-B-C+D).

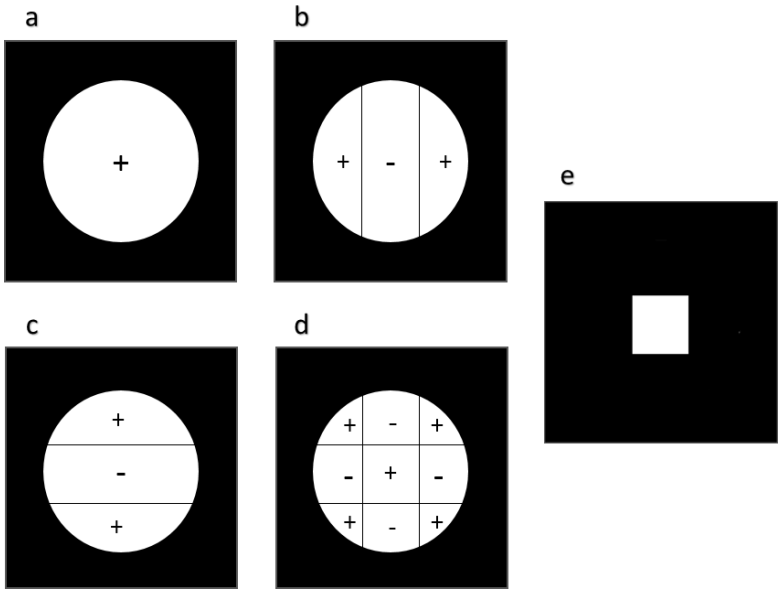

Fig 12 Experimental evaluation of 2D ISIS localization by MRI. (A) Image representation of a water-filled sphere. No spatially selective (in-plane) inversion pulses were executed. (B and C) Images (in absolute value) in which one spatially selective inversion pulse has been executed. The + and− signs correspond to noninverted and inverted areas, respectively. (D) Image of the sphere after the execution of two spatially orthogonal selective inversion pulses. Due to the double inversion in the middle of the sphere, the magnetization resides along the positive longitudinal axis. (E) The localized volume is obtained according to the following add–subtract scheme : (E) = (A) − (B) − (C) + (D).

Because of the way it is sequenced, ISIS leads to the possibility of using very short TE times [14], which greatly benefits the identification of short T2 species (such as ATP with 31P MRS).

The practice of Outer Volume Supression (OVS) is consistently used in combination with the ISIS sequence, giving birth to (Connelly et al [15]) a new sequence named OSIRIS (outer volume suppressed image related in vivo spectroscopy). The frequency domain excitation profile of a noise pulse consists of a selective null band in which magnetization is not perturbed outside this null band. This combination leads to a significant suppression of magnetization outside the VOI, such that the receiver gain and motion problems are minimized. Even though noise pulses are most commonly used for this effect [15], any kind of OVS can be used [14].

Even so, ISIS comes with problems of its own. In vivo MR Spectroscopy scans (and particularly in 31P spectroscopy even more so) are often executed using surface coils for increased sensitivity, but that comes with a cost. B1 magnetic field inhomogeneity can degrade the performance (slice profile) of the inversion and excitation pulses, leading to greatly reduced sensitivity (complete opposite to the initial intention of using surface coils), and increased contamination from unwanted signals [45].

5.2 Single Pulse and 1D acquire (SPULS)

Regarding non-localized spectroscopy, SPULS is probably one of the simplest methods one can use. Although it's almost exclusively recommended by Agilent as a test sequence to check the NMR signal during calibration [46] (possibly because of its reduced flexibility in tinkering with parameters), its speed and high SNR are rather positive aspects to be considered.

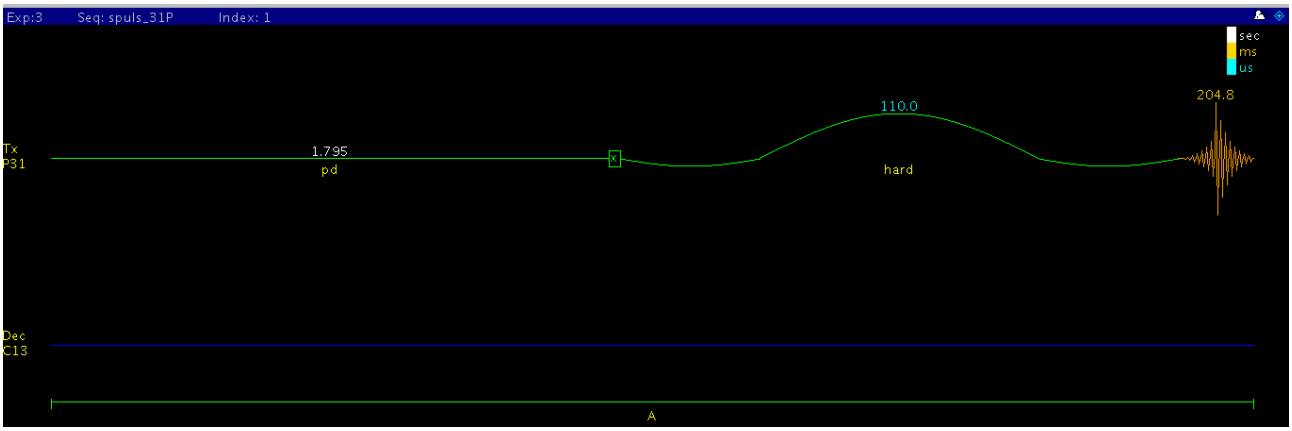

Fig 13 SPULS pulse program, as seen in vNMRj

Measurement of regular 1D NMR experiment is extremely simple and usually carried out in three stages: The sample/subject reaches equilibrium; An rf signal of sufficient power is transmitted and for a sufficient period of time (only a few microseconds, as localization is not needed), in order to move the magnetization vector from the z-axis to the x,y-plane (a pulse of up to 90°).

The signal that evolves due to precession of the magnetization vector is measured after the pulse and at the end of the process, the vector returns to equilibrium on the z-axis (process known as FID).

Possibly the biggest problem one comes across when using the SPULS sequence aimed at actually gathering valuable spectroscopy information in an in vivo setting is the intrinsic inhomogeneity in living structures. Due to the lack of localization, all acquired information is referent to the sample/body as a whole, with no information whatsoever on where the signal is coming from.

Without the use of localization, scan speed times increase and signal loss becomes minimal, meaning an improvement for SNR. Still, as of now this technique is apparently useless for this matter, since without localization there's no way of knowing where the signal originates from, and the observed sample/subject is not a homogenous structure. Luckily, this problem can be circumvented using OVS. By saturating the unwanted structures (skin, muscle, fat) prior to the actual SPULS sequence, signal from outside our region of interest can be theoretically avoided, with the remaining signal coming from the desired structure.

Alas, use of outer volume suppression with this sequence is not supported out of the box, meaning it had to be hard coded into a new sequence (SATSP), compiled and only then it is ready to run.

Each new modification in the desired parameters, albeit small, requires the user to go back and forth different sequence layouts, namely SPULS and PRESS, in order to access all parameters that need changing. In retrospective, it would have been wiser to build a proper GUI for this specific sequence, which would streamline the process, making it faster and easier to use.

5.3 Saturated Single Pulse (SATSP)

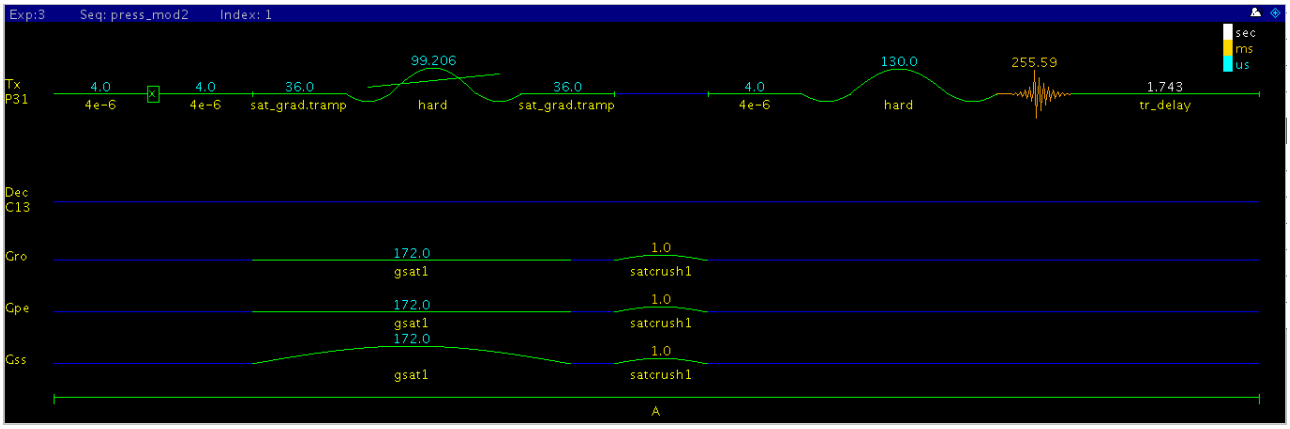

Fig 14 SATSP pulse program, as seen in vNMRj

Essentially, this sequence consists on the SPULS sequence program preceded by a saturation pulse, of whatever nature we may choose. The basic idea is to saturate the unwanted region prior to the excitation pulse and acquisition, so that we only acquire signal coming from the non-saturated region, ie. our region of interest. The main advantage would be the simplicity and fast acquisition times. As a main disadvantage, this sequence only provides 1D localization.

This sequence was achieved by combining existent Varian code used in both SPULS (for the excitation pulse) and PRESS (for the saturation pulses) pulse sequences, with some modifications. The complete pulse sequence code can be found at the end of this dissertation, with the code properly commented and described.

5.4 Chemical Shift Imaging (CSI)

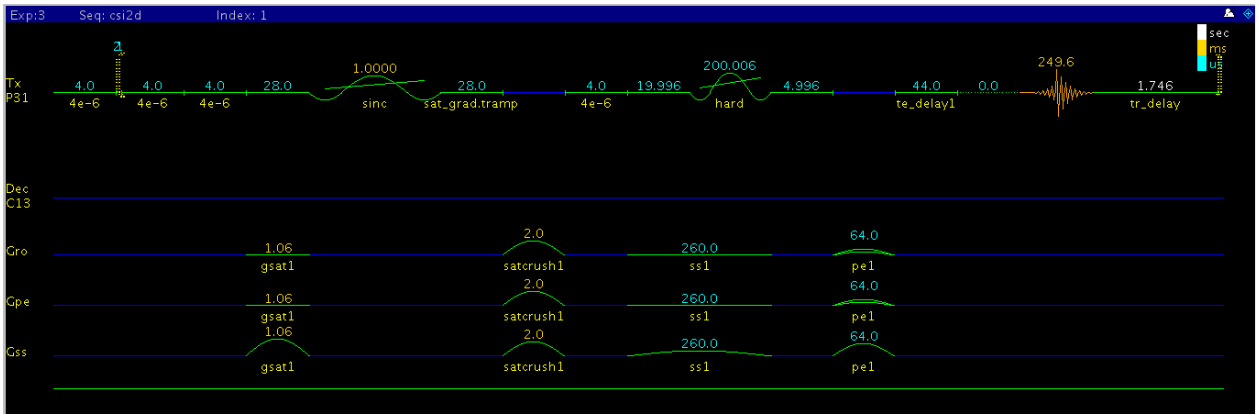

Fig 15 CSI pulse program, as seen in vNMRj

Also referred to as Metabolic Imaging, CSI consists in recording the spectroscopic data for a group of voxels, in slice(s) (2D) or by volume (3D). It is based on a repetition of PRESS type sequences to which is added spatial phase encoding. The number and direction of phase encodings depend on the number of dimensions explored (be it 1D, 2D or 3D), adding on to acquisition time. Signal processing calls on Fourier transforms (1 for each phase-encoded dimension phase + 1 for spectral analysis) and requires data correction (correction of the baseline, phase, etc).

The results appear in the form of parametric images (metabolic maps) or a matrix of the spectra of the regions to be studied.

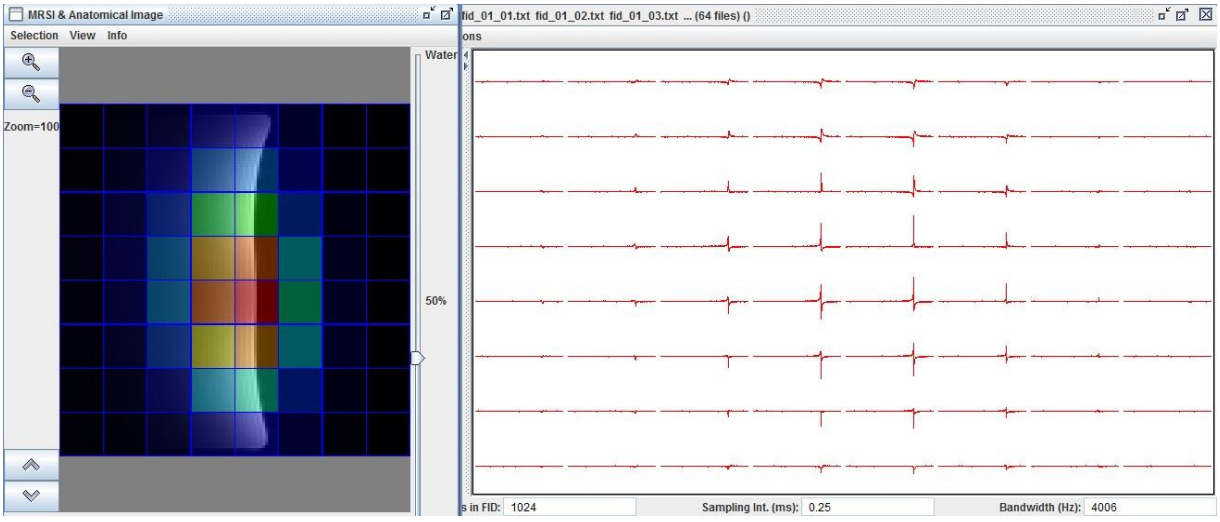

Fig 16 CSI map and relative anatomical representation. Each voxel represented on the figure (PPA phantom SCOUT acquired image) on the left has a correspondent spectrum on the right, creating a metabolic matrix.

The PRESS localization method [14] is a so-called double spin-echo method, in which slice-selective excitation is combined with two slice-selective refocusing pulses. When the first 180° pulse is executed after a time t1 following the

excitation pulse, a spin-echo is formed at time 2t1. The second 180◦ pulse refocuses this spin-echo during a delay 2t2, such that the final spin-echo is formed at time 2T1 + 2T2 (which equals the echo-time of PRESS, i.e. TE = 2T1 + 2T2). The first echo contains signal from a column which is the intersection between the two orthogonal slices selected by the 90◦ pulse and the first 180◦ pulse. The second spin-echo only contains signal from the intersection of the three planes selected by the three pulses resulting in the desired volume. Signal outside the VOI is either not excited or not refocused, leading to rapid dephasing of signal by the 'TE crusher' magnetic field gradients.

5.5 Gradient Echo (GEMS)

GEMS (Gradient Echo Multi Slice), the gradient echo sequence illustrated in Fig 17 operates in a similar way to the spin echo sequence, although uses bipolar gradients rather than an inversion pulse to achieve refocussing and echo generation [48]. Generally, smaller flip angles (for example, 30°) are used than in a spin echo sequence; this means that less signal will be available for image generation, but allows residual z magnetization to be consumed in subsequent excitations – thereby allowing sorter repetition times and faster image acquisition. Although z magnetization does not fully recover due to the short repetition time, equilibrium is established after the first few excitations. Gradient echo imaging generally allows faster acquisition with lower SAR than spin echo sequences, albeit somewhat more vulnerable to certain artifacts (including those due to field inhomogeneities). Variations on the sequence allow improvements in terms of signal strength, artifact reduction, imaging time and measurement of flow.

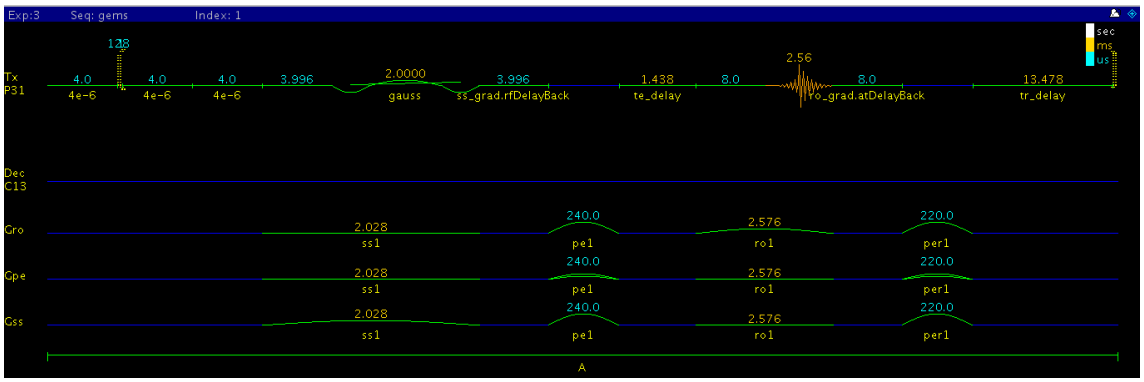

Fig 17 GEMS pulse program, as seen in vNMRj

GEMS is a default pulse sequence present in Varian scanners that uses a changeable flip angle instead of a 90° pulse and a gradient instead of a RF pulse to rephase the FID. T2*, T1 weighted and proton density images can also be acquired using this specific sequence. The flip angle in combination with the TR determines the T1 weighting and the TE controls the amount of dephasing.

6. Experimental Protocols

Several Experimental protocols, each for a specific purpose, were followed throughout the course of this study. Here you can find protocols for both phantom and in vivo use that more or less acted as guidelines for each experiment. The required preparation and handling of every animal used during this study was performed by an experienced member of the Edinburgh Preclinical Imaging Centre, diligently following every normative guideline.

6.1 Phantom Protocol

1) Starting with positioning, the combined Doty 1H/31P coil should be centered relative to the phantom (if the Liver Phantom is being used, the small compartment should face the surface coil). It should be ensured that the phantom is leakproof so that no damage may occur to both the coil and the machine.

2) Perform coil tuning and matching. Register values for future reference.

3) SCOUT images should be acquired to verify the correct position of the phantom. If the correct position is not achieved at first, adjust it accordingly, repeat SCOUT image acquisition and coil tuning/matching if necessary until the desired position is achieved.

4) Proceed to 1H power calibration and register the values for further reference.

5) When using the Liver Phantom, acquire SCOUT images with progressively higher flip angles. Obtained images where the second compartment appears brighter mean that a 90 degree flip angle (or close to it) is most likely affecting that area. Register those values.

6) In order to achieve the best possible shimming, a few different methods can be applied:

    a) Automated Shimming

        i) Global shim techniques, such as quickshim can be used. While using the Liver phantom, it should be very important to choose a FA value that works in our favour, with more signal coming from our region of interest.

        ii) Localized shim techniques, such as ge3d, can also be used. Shim gradient values will be chosen in accordance to the user defined voxel.

    b) Manual Shimming

        i) Global shimming can be done by loading a regular SPULS sequence. Again, carefully choosing a favorable FA is vital to achieve a good result. Signal should

be, as much as possible, coming from our area of interest, and not any surrounding areas.

ii) Localized shimming can be done by loading a PRESS sequence, selecting a voxel of interest and varying the shim gradient values until the desired result is achieved.

7) Using the Liver Phantom, 31P power calibration should be done in accordance to the Phenylphosphonic Acid peak, originating from the second compartment, further away from the coil. For single compound/peak phantoms, power calibration is straightforward, as only that peak can be considered. Register values for further reference.

8) The phantom is now ready to be scanned. Choose the adequate sequences and parameters that fit your purpose in the experiment.

6.2 In Vivo Protocol

1) Animal must be anesthetized before being put in the scanner. A rectal thermometer is used to check the subject's temperature and a surface electrode placed directly below the subject's chest to monitor the heart rate.

2) Concerning positioning, the animal is placed on the animal holder and the combined Doty 1H/31P coil should be centered relative to the liver of the animal. Tape can be used to maintain it still and minimize the effects of respiratory movements.

3) After the subject is Coil tuning and matching.

4) SCOUT images should be acquired to verify the correct position of the subject. If the correct position is not achieved at first, adjust the subject accordingly, repeat SCOUT image acquisition and coil tuning/matching if necessary.

5) 1H power calibration.

6) SCOUT images with progressively higher flip angles should be acquired. Obtained images where the liver is brighter mean that a 90 degree flip angle is most likely affecting that area.

7) In order to achieve the best possible shimming, a few different methods can be applied:

    a. Automated Shimming

i. Global shim techniques, such as quickshim can be used. In this case, it should be very important to choose a FA value that works in our favour, with more signal coming from our region of interest, the liver.

ii. Localized shim techniques, such as ge3d, can also be used. Shim gradient values will be chosen in accordance to the user defined voxel.

b. Manual Shimming

i. Global shimming can be done by loading a regular SPULS sequence. Again, carefully choosing a favorable FA is vital to achieve a good result. Signal should be, as much as possible, coming from our area of interest, the liver, and not the muscle or any surrounding areas.

ii. Localized shimming can be done by loading a PRESS sequence, selecting a voxel of interest and varying the shim gradient values until the desired result is achieved.

8) 31P power calibration should be done in accordance to the Phosphocreatine peak (PCr), with this signal coming from the muscle region, closer to the coil.

9) The animal is now ready to be scanned. Choose the adequate sequences and parameters for your specific purpose.

7. Methods of Data Analysis

While there are several options on the market for MR Spectroscopy analysis, namely LCmodel or even Matlab, jMRUI was chosen. jMRUI (short for Java-based Magnetic Resonance User Interface) is a software package used for processing of MRS and MRSI data. It includes algorithms for frequency selective filtering of signals, correction of eddy current artifacts, Cadzow signal-to-noise enhancement, linear prediction, non-linear fitting, etc. It is mainly developed as part of Marie Curie Framework by the D. Graveron-Demilly group at the Claude Bernard University Lyon 1 in France. The software is not open-source, but licenses are free for academia, on the condition that they register on the website.

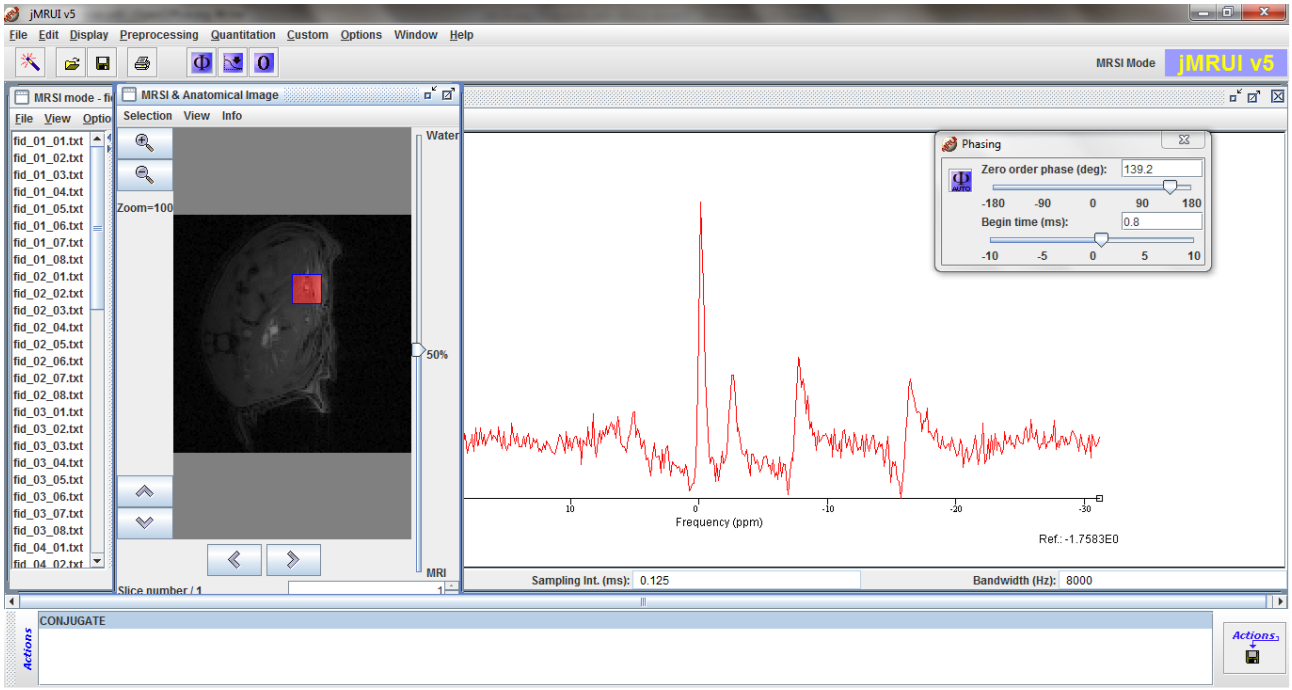

Fig 18 General view of jMRUI. A CSI sequence is displayed, where we can see the anatomical image and the selected voxel, the correspondent spectrum as well as a Phase Parameters toolbox

7.1 Preparation

Before starting to quantify the metabolites present in the spectra, one has to prepare the data for analysis. This procedure includes several steps, detailed below.

The first thing to do is reversing the spectrum (conjugate signal). Raw MR Spectroscopy data acquired in Varian scanners is not automatically presented according to the MR Spectroscopy standard. To fit this standard, one has to reverse the spectra in order to fit the metabolites in the expected frequency range when displayed as PPM.

Next up, comes Apodization, literally meaning "removing the foot", is the technical term for changing the shape of a mathematical function, an electrical

signal, or anything equivalent. It is commonly used in signal processing, usually by means of applying the Hann window in the Fast Fourier transform in order to smooth the discontinuities at the beginning and end of the sampled time record. In purely aesthetic terms, it makes the spectrum appear to be smoother, reducing (or even removing completely. Depending on the degree of apodization) the sharp angles present in each peak. This tends to erase the visual noise usually present in MR Spectroscopy spectra

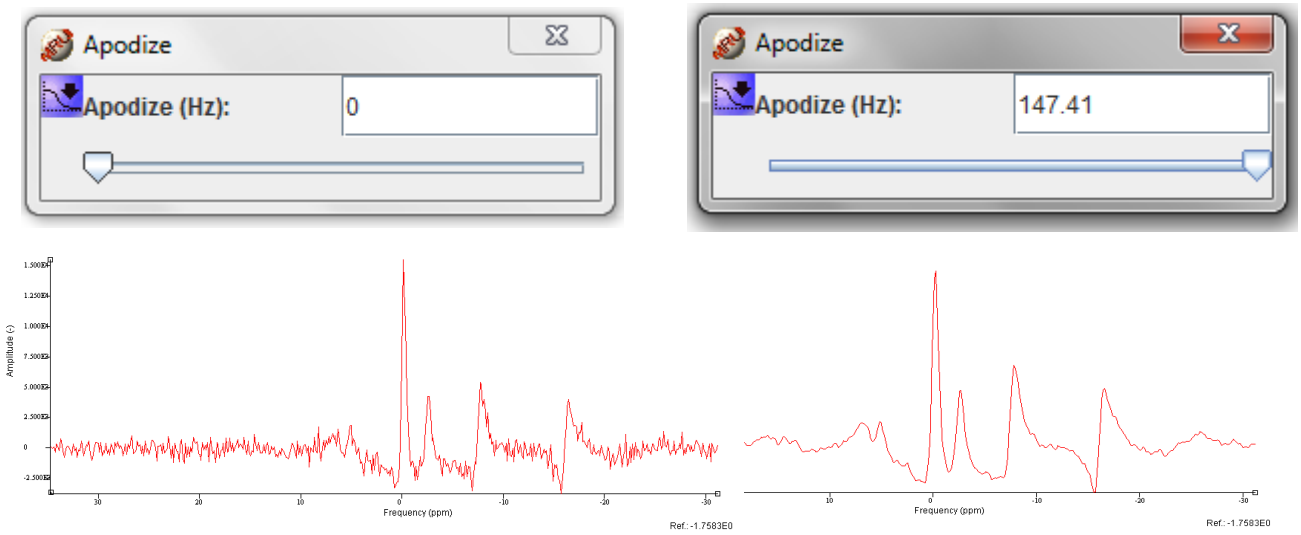

Fig 19 *Apodization Toolbox and its effect on the visual representation of a spectrum. No apodization was used on the left spectrum, as evidenced by the apparently erratic variations, and extreme apodization was used on the spectrum on the left, now displaying very smooth lines*

While the visual effect of apodization is easy on the eyes, it also means one can lose information if used in a careless manner. Luckily, jMRUI presents the option of looking at the apodized data while the analysis is done using the unedited data instead of the apodized one.

The Zero Order Phase parameter is pretty much self-explanatory, as it allows for user to adjust the phase of the signal to better fit the desired interest (pretty much common ground on any signal processing tool available). Due to the intrinsic nature of surface coils (B1 inhomogeneity), this parameter needs to be constantly adjusted to avoid phase issues, as different voxels are affected by different Flip Angles.

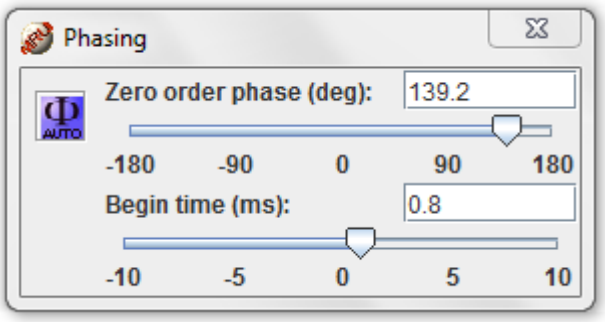

Fig 20 Phasing Toolbox, showing both Zero Order Phase and Begin Time as flexible parameters.

In regards to the Begin Time parameter, its benefits may not be as easy to see. Essentially what it does is it cuts out a determined amount of points at the beginning of the data set. This helps solving some major phasing issues.

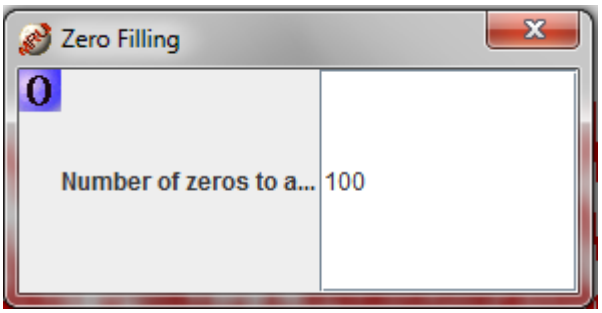

Fig 21 Zero Filling Toolbox, with the number of points to add to the spectrum.

Zero filling is another tool to take into account. It allows one to use a longer FFT, which will produce a longer FFT result vector. A longer FFT result has more frequency bins that are more closely spaced in frequency. This might result in a smoother looking spectrum when plotted without further interpolation.

Although this interpolation won't help with resolving or the resolution of and/or between adjacent or nearby frequencies, it might make it easier to visually resolve the peak of a single isolated frequency that does not have any significant adjacent signals or noise in the spectrum. But, essentially, zero padding/filling before a DFT/FFT is a computationally efficient method of interpolating a large number of points.

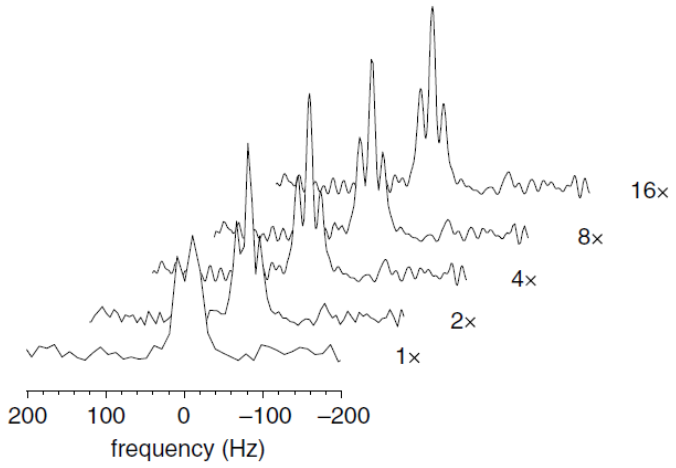

Fig 22 Effect of zero filling on spectral resolution. The triplet resonance Beta-atp is not well resolved after a FT of the acquired data points. Zero filling the original data (by a power of 2), completely resolves the triplet resonance. After four times zero filling no further improvement in spectral resolution is observed (this, of course, on a case by case basis) [14]

7.2 Quantification

And then comes the actual data quantification. For medical diagnosis or biochemical analysis accurate and efficient quantification of magnetic resonance spectroscopy signals is of the utmost importance. However, these signals are often characterized by a low SNR and overlapping peaks, which means that simple signal processing methods such as numerical integration, are all but useless in this field. Starting in the mid-90's, a number of more advanced time domain techniques based on a mathematical model function have been developed [49].

Non interactive methods exist that are computationally efficient and fully automatic. Among these are the very popular SVD (singular value decomposition) and LP (linear prediction) methods, as well as all their variants. Still, a serious drawback is the fact that only very limited prior knowledge can be incorporated in these algorithms and that the model function is restricted to a sum of complex exponentially damped sinusoids. On the other hand, interactive methods exist that provide more user involvement, and do allow the inclusion of a robust amount of prior knowledge, even if they are computationally less efficient.

7.2.1 AMARES

AMARES (Advanced Method for Accurate, Robust and Efficient Spectral fitting), is one of these methods. As defined by its creators, AMARES is an improved interactive time domain method for accurate and efficient parameter estimation of MR Spectroscopy signals with use of prior knowledge. It uses a version of NL2SOL, a sophisticates nonlinear least-squares, which can be adjusted based on prior assumed knowledge. AMARES was first brought up as an alternative to VARPRO, which uses a simple Levenberg-Marquardt algorithm to minimize the variable projection functional. Its performance was confirmed to be superior to VARPRO in terms of accuracy, robustness, and flexibility, in both in-vivo and simulated experiments [49][50]. AMARES is, by definition, dependent on user interaction, which means that the more information the user itself has when analyzing the data, the better. With this in mind, as a way to aid in spectra visualization, every acquired spectrum was apodized.

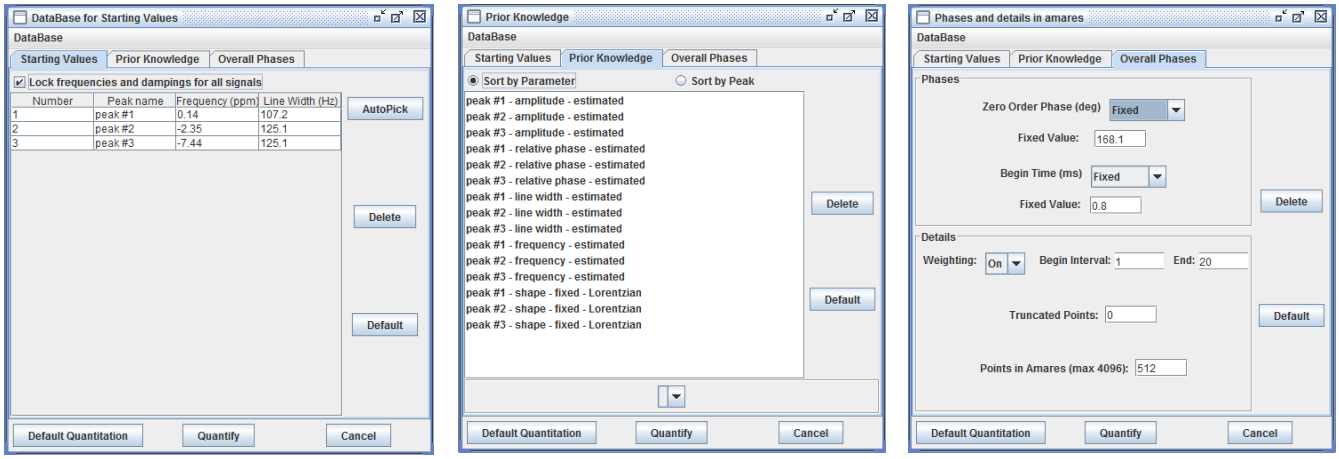

Fig 23 A three way view of the AMARES toolbox as presented in jMRUI, displaying the three main parameter categories at our disposal, "Starting Values", Prior Knowledge" and "Overall Phases", from left to right

Weighting is the multiplication of the first points of the signal, the FID, with a quarter-sine wave. This operation is useful in the quantitation of a signal with a large background signal, or if the FFT of the signal has a bulgy baseline (both usually happen in 31P MR Spectroscopy). For the same reasons, the first points of the FID could be truncated. Truncation of points does not imply physical truncation of the original signal. The quantitation will be performed without the number of points indicated in this field. According to jMRUI's manual, weighting can change the estimated amplitudes for components to about 20% for an interval from the 1st to the 20th point and that truncation can throw away valuable information in the signal, and is meant to be used carefully. In the details field, the number of points used in AMARES can be chosen also.

Prior Knowledge					Phases		Details		
Amplitude	Line width	Relative phase	Frequency	Shape	Zero Order Phase	Begin Time	Weighting	Truncated points	Number of Points
Estimated	Estimated or bound by soft constraints	Estimated	Estimated or bound by soft constraints	Usually Lorentzian	Fixed during the analysis of each voxel. Variable between voxels.	Fixed	On	Usually 2	Maximum, dependent on the acquire data set.

Table 2 Typical values/settings used in each of the AMARES required parameters

The parameters described above are merely representative of the typical settings used within AMARES, and can be altered and improved in relation to specific cases. Luckily, AMARES provides visual aid for this case, displaying both the original and estimated signal side by side for an easy comparison. This way, it is possible to quickly assess if the analysis is working as intended (even if on a purely visual perspective only) and decide whether to move forward with the analysis or to go back and modify some of these parameters to better suit the acquired data.

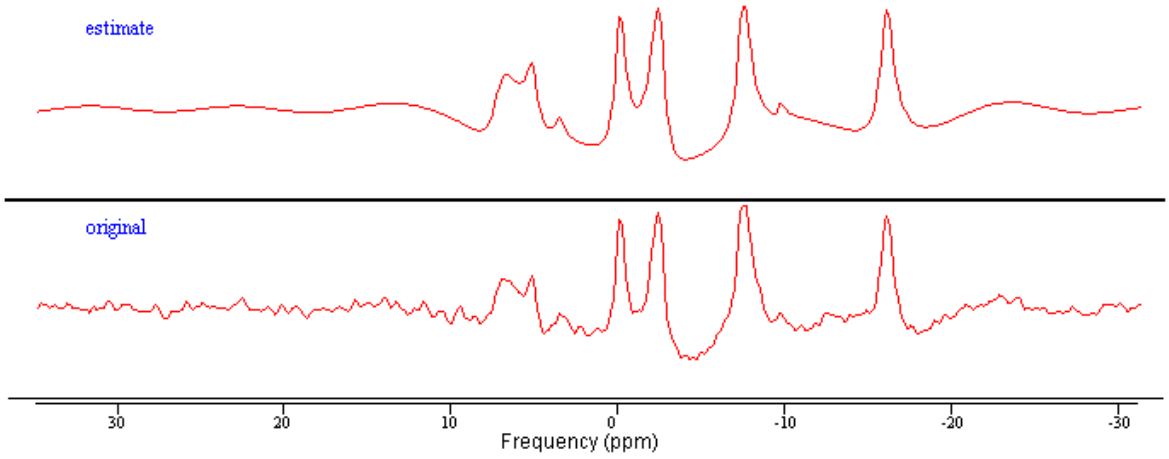

Fig 24 Example of good data fitting using Amares. Estimated spectrum looks similar to the original one.

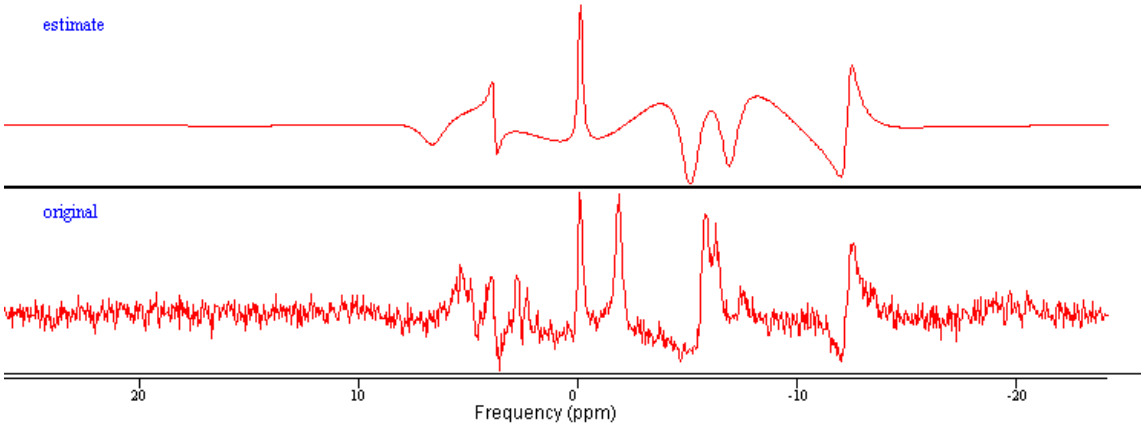

Fig 25 Example of bad data fitting using Amares. Estimated spectrum barely resembles the original.

In the first case, the estimated signal almost precisely matches the one from the

original acquisition. This is the preferred case, as the quantified data will resemble actual acquisitions more closely (residue will be minimized). On the second figure, we are presented with a much noisier spectrum. There are now large discrepancies between the original and estimated spectra, such as unusually wide peaks, mysterious slopes around the -5 ppm area, and general phase issues. This means that AMARES is not doing its jobs properly, and estimation needs to be redone using a different approach within AMARES itself. The estimated components are shown in a much smoother display due to the lack of noise.

Note: There were a number of recurrent bugs found within jMRUI.

The first one relates to the AMARES analysis itself. If the AMARES dialog window is closed during a work session, several problems might occur. These problems range from the inability to select peak line width or automatically selecting several peaks at once, downright to displaying seemingly wrong values during data analysis. Once these problems start to appear they remain present until a new session is initiated. This can be circumvented by not closing the AMARES parameter box between the analysis of different voxels, and merely putting it in the background while the user changes the rest of the parameters.

Another has to do with some data sets that were acquired using the CSI pulse sequence. Jmrui is supposed to automatically detect several parameters inherent to the acquired data, such as the Sampling Interval, Bandwidth, Transmitter Frequency and Main Magnetic Field. While most times these parameters are rightfully displayed, data acquired using CSI has this problem. The correct values need to be manually inserted, otherwise data analysis is meaningless, as the results will take into consideration wrong prior knowledge.

8. Phantom Design

8.1 Liver Phantom

Before the actual in-vivo scanning takes place, MR Spectroscopy sequences need to be chosen, tested and optimized to prevent the use and subsequently needless killing of rodents for academic only purposes. Among the more common alternatives are both the use of already deceased animals (ex-vivo studies), or the use of replacement phantoms.

8.1.1 Concept and early draft

So, the creation and subsequent MRS scanning of a rodent phantom that comprises a "skin/muscle/fat" + liver slice came to fruition. This phantom would be primarily used to test and assess the viability of a number of MRS sequences, optimize its parameters and a get a better perception of the maximum viable scanning "depth". This way, the chosen sequence(s), and its parameters will hopefully have little left to be optimized during the in vivo scan time (relatively speaking), leading to a faster and trouble free experimentation. Still, not all parameters can be fully optimized using a phantom. The schematic in Fig 26 seen here is to be a visual representation of said “skin/muscle/fat” + “liver” phantom, as well as the relative positioning of the surface coil.

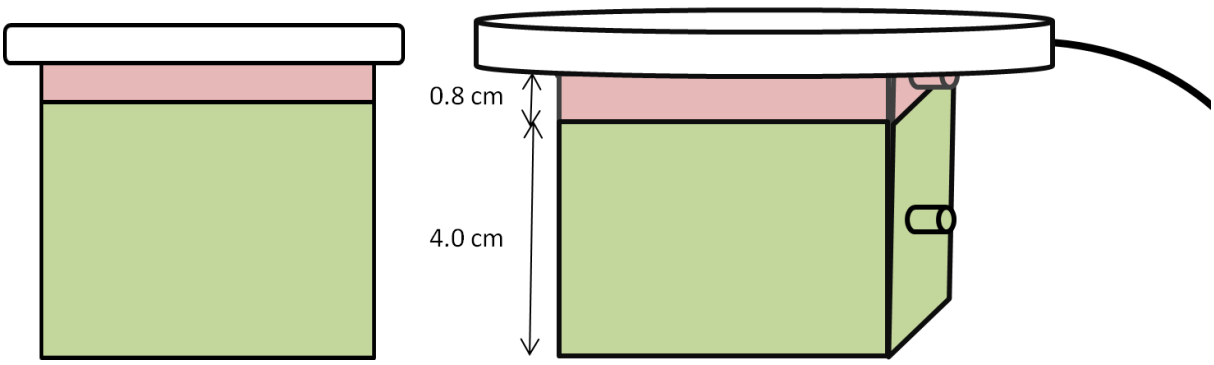

Fig 26 Early draft of the Liver Phantom. On the left, a sideway cut of both compartments and the surface coil on top. On the right, isometric perspective of the Liver Phantom with the surface coil on top.

The two compartments that this phantom depicts have significant differences, both anatomically (in this case, regarding the thickness/depth of each layer), and physiologically (regarding the content of each compartment, in terms of specific metabolite presence and ratio).

Starting by the most outward layer, skin thickness in rats varies a lot with age but remains mostly within small consistent boundaries when oldness is not an issue (Changes in Electrophysiological Properties of Rat Skin with Age). In this sense, if a greater attention to detail is required, the skin compartment’s thickness could be depicted in accordance to the average age of the rats that will be used later in

the in-vivo experiments. In terms of muscle and fat layers, their average thickness tends to vary a lot with various outside factors such as food intake, exercise or even stress [51]. Taking into account several MR scans of common Sprague Dawley rats, an average thickness of 0.8 cm was decided for the first compartment of the liver phantom. In terms of metabolite concentration, studies consistently show that low ratios of phosphocreatine (PCr) to adenosine triphosphate (ATP), high levels of phosphomonoester (PME), Pi, and phosphodiester (PDE) relative to PCr, are present in rat skin [51]. When it comes to muscle composition, Phosphocreatine (PCr) is the most characteristic and easily identifiable metabolite, being present in high concentrations in the muscle and almost totally absent from both the skin and liver [4], quite useful for voxel bleed localization. The second and final layer of the phantom corresponds to the "liver" compartment. In this layer, thickness is not particularly relevant as long as it's guaranteed to exceed the maximum viable range of the phosphorous surface coil (it is a prior assumption that the average liver thickness, combined with the previous layer above will largely exceed it, so it is not a problem here). Even so, to ensure some consistency, the thickness of this layer should be in accordance to the average liver thickness of a rat of similar age to the ones that will be used in the *in-vivo* MRS. Liver phosphorous metabolite composition is fairly simple, and usually consists of 6 (relevant) different components ranging 4 distinct metabolites: PME, phosphomonoesters; Pi, inorganic phosphate; PDE, phosphodiesters; and ATP (alpha, beta and gamma peaks).

8.1.2 Phantom Design and Production

Now that the general idea of what the Liver Phantom should be like was set, there was the need to actually design it and build it. Although the phantom design was quite simple in nature, it was also very specific. It was absolutely necessary for it to have two separate compartments, be easy to fill with a liquid substance and as leak-proof as possible. The desired features, while somewhat flexible, were not so common that you could simply find a container with more or less those characteristics in your everyday life. For this reason, 3D printing was thought of as the most suitable approach.

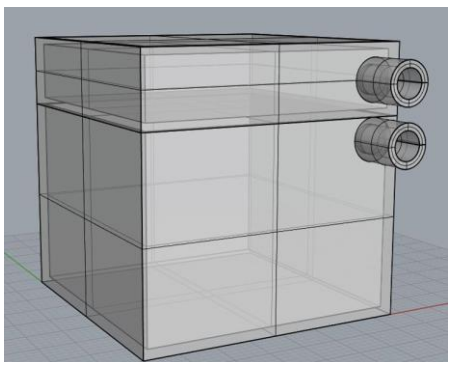

Fig 27 First tridimensional draft of the Liver Phantom. Both compartments are already in place, design is not final